Acta Astronautica 236 (2025) 882–896

Contents lists available at ScienceDirect

Acta Astronautica

journal homepage: www.elsevier.com/locate/actaastro

Research paper

Approximated methods for the analysis of the unsteady shock wave motion in inlet unstart processes

Carlos Carbajosa *, Ángel Sanz-Andrés, Alejandro Martínez-Cava, Sergio Marín-Coca, Sebastián Franchini

Instituto Universitario "Ignacio Da Riva" (IDR/UPM), Universidad Politécnica de Madrid, Plaza Cardenal Cisneros, E-28040 Madrid, Spain

ARTICLE INFO

Keywords:
Unstart
Motion speed
Shock-wave
Ramjet/scramjet
Shock-train
Pseudo-shock

ABSTRACT

The behavior of shock waves in supersonic and hypersonic inlets is instrumental in the operation of ramjets and scramjets, as it is critical for preventing undesired phenomena such as unstart and buzz. Studying the evolution of shock waves within the inlet duct is essential for understanding these phenomena. This work presents approximated solutions to the novel and recently published DS^2M (*Duct Shock Speed Model*), which allows for the estimation of normal shock motion speed, the identification of equilibrium positions, and the equilibrium positions stability analysis. Although the DS^2M model has been validated through experimental comparisons, its numerical resolution and complexity hinder preliminary design analysis and rapid calculations. In this study, simplified models are introduced, providing straightforward analytical expressions to evaluate shock wave dynamics valid in the Mach-close-to-unity range (which is a common incident Mach number range for normal shock waves to appear in the design of engine inlets). The approximations developed here facilitate the identification, during the early stages of design, of key parameter influences. The proposed formulations allow for rapid and reliable assessment of motion speed, equilibrium positions, and stability, providing explicit expressions avoiding the need for advanced computational tools such as nonlinear solvers. Within the range of validity of the simplified DS^2M models, the results demonstrate good agreement with the full model. This work provides analytical tools for the preliminary design of supersonic and hypersonic inlets, extending the capabilities of the original model, and explicitly showing the influence of design parameters on shock wave dynamics in the Mach number range considered.

1. Introduction

1.1. Conceptualization and previous research

The swallowing and expelling of shock waves in supersonic or hypersonic inlets are some of the fundamental phenomena involved in the operation of ramjets and scramjets. In this regard, excessive heat from combustion can cause thermal choking, reducing the Mach number to unity and disrupting the flow [1,2]. This problem also applies to other phenomena, such as the unstarting of supersonic inlet cascades [3]. Ramjets and scramjets rely on inlets for optimal mass flow and pressure recovery across a number of mission conditions, operating in a stable started mode to avoid unstart [4–6].

Unstart occurs when internal shock waves are expelled, resulting in a detached shock upstream of the inlet entrance and the associated inlet spillage. Factors influencing unstart include flight Mach number, contraction ratio, geometry, and operational conditions like inlet angle of attack, fuel addition, overheating, and back-pressure [5,7–9]. Shock stability depends on its equilibrium position, which depends on the inlet duct converging or diverging geometry, leading to regions of stable or unstable configurations defined by contraction ratio and Mach number [4,10–12]. There are two stable configurations: swallowed shock wave placed at the diverging part of the duct, or expelled shock wave placed at some distance in front of the inlet entrance.

The key operational limits are the Kantrowitz-Donaldson limit (KD, see Fig. 1), and the isentropic limit (IS). The KD limit defines the condition for the autonomous swallowing of a shock wave when the throat is choked (shock wave just at the entrance, subsonic flow in the converging part with choked throat). The isentropic limit (IS), defines the minimum threshold for a shock-free sonic throat operation (supersonic flow in the converging part, and choked throat). Intermediate configurations between KD and IS limits depend on the previous flow history, thus leading to hysteresis phenomenon [11].

* Corresponding author.
E-mail addresses: c.carbajosa@upm.es (C. Carbajosa), angel.sanz.andres@upm.es (Á. Sanz-Andrés), alejandro.martinezcava@upm.es (A. Martínez-Cava), sergio.marin.coca@upm.es (S. Marín-Coca), s.franchini@upm.es (S. Franchini).

https://doi.org/10.1016/j.actaastro.2025.07.026
Received 4 June 2025; Received in revised form 30 June 2025; Accepted 11 July 2025
Available online 23 July 2025

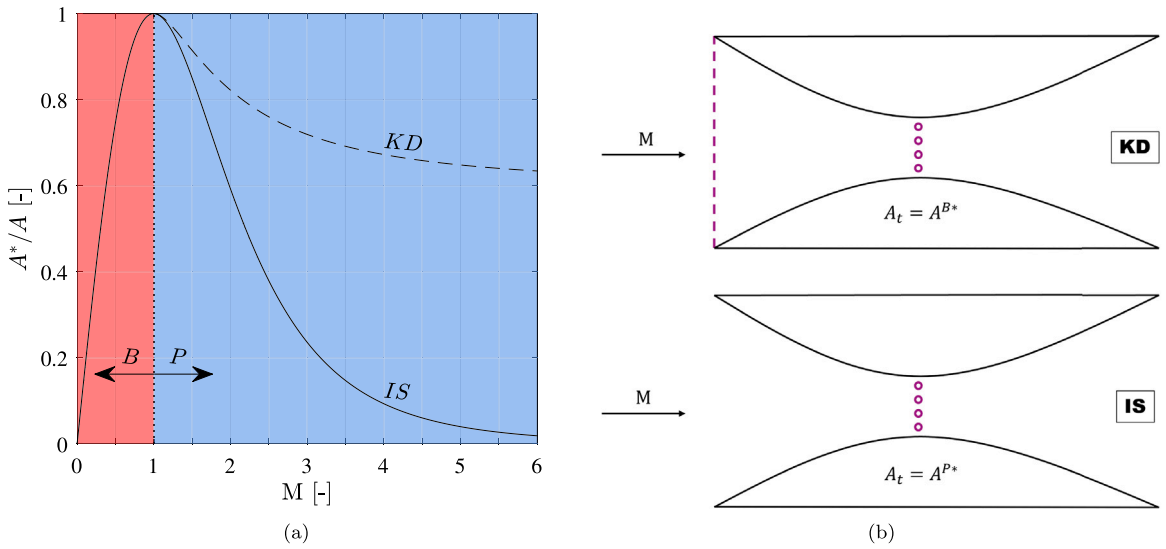

Fig. 1. (a): Variation of the contraction ratio, $CR = A^*/A$, as a function of the Mach number of the incoming flow, M. Isentropic limit (continuous line, IS) and the Kantrowitz-Donaldson limit (dashed line, KD). Vertical dashed line at M = 1: boundary between the solution for the subsonic branch (left red region, B) and the supersonic branch (right blue region, P) [11]. Adapted from [13]. (b): Kantrowitz-Donaldson (KD) and isentropic (IS) limits flow patterns schematic representations. The vertical dashed line represents the shock wave, while the dotted line corresponds to critical conditions at the throat.

Recent work has investigated suppression techniques for hysteresis in mixed-compression inlets, including the use of distributed bleed systems to stabilize the throttling/unthrottling process [14]. For single-throat inlets, configurations transition takes place between started and unstarted modes at these limits. Multi-throat systems, such as those provided with flow control valves, add complexity to the previous picture, introducing multiple stable flow patterns and stability changes [15].

Various models have been developed in order to analyze shock wave behavior in ducts. Some of the most remarkable contributions in this field are:

- Kantrowitz and Donaldson: Foundational work on shock stability and throat conditions [10,16].
- Whitham's CCW Method: Studied shock motion in ducts with stationary or flowing mediums [17].
- Han and Yin: Extended CCW methods to moving fluid scenarios [18].
- Tahir: Adjusted the KD limit for oblique shocks, expanding applicability [19].
- Carbajosa, Sanz-Andrés, Martínez-Cava and Ogueta-Gutiérrez: Presented a simplified model, the DS^2M (*Duct Shock Speed Model*) model, for the shock motion speed determination, equilibrium locations identification and stability assessment [13].

In these models, complexities like acoustic effects are often neglected, which is valid if shock wave motion speed is low enough.

In hypersonic inlets, normal shocks are replaced by pseudo-shocks (a train of interacting shocks, known as shock-train, followed by subsonic deceleration). These configurations are stabilized using isolators, which mitigate oscillations caused by interactions between boundary layers and shock waves [1,11]. Pseudo-shock pressure jump can be modeled by adapting normal shock equations, accounting for friction and area changes [20,21]. During unstart, supersonic flow at the duct disappears, thus pseudo-shocks can no longer exist, leading to spillage and reduced mass flow. Unsteady processes dominate this transition, marked by abrupt pressure changes in the subsonic region [22]. Experimental studies have further characterized the stability margins of variable-geometry combustors, highlighting the impact of geometry and equivalence ratios on stability in wide operational domains [12]. Additionally, active flow control methods—such as localized energy deposition—are being investigated for their ability to enhance inlet performance, mass flow capture, and total pressure recovery [23]. Porous-wall configurations have also been introduced in rotating detonation combustors to suppress inlet blockage and extend stable operating ranges [24].

This framework serves as the base for studies on shock dynamics and provides guidance for the design of inlets in high-speed flight applications. In constant or slowly varying section ducts, there is an interaction between the generated shock waves and the boundary layers that appear near the walls. Under these conditions, normal shock waves naturally occur only for Mach numbers close to unity—up to ≈ 1.2 [25]. For higher Mach numbers, viscous effects tend to generate shock waves with a λ or χ shaped structure [25]. For even higher Mach numbers, the flow patterns typically involve oblique shocks with multiple reflections, a phenomenon already discussed in the previous paragraph referred to as a pseudo-shock, which consists of a shock-train followed by subsonic deceleration, as shown by Gnani, Zare-Behtash and Kontis [25]. At these higher Mach numbers, there exists an equivalence between a pseudo-shock and a normal shock wave subjected to a corrected incident Mach number lower than the original [21]. Therefore, these facts justify the interest in studying the behavior of normal shock waves in a simplified manner (specifically in terms of motion speed, equilibrium positions, and stability) for Mach numbers close to unity. This study relies on simplifications of the DS^2M model for Mach numbers close to unity, which is in accordance with the fact that either these conditions occur naturally or they are used to approximate the behavior of more complex structures (such as pseudo-shocks modeled as a normal shock subjected to a reduced effective Mach number). In the simplified analytical expressions obtained, the influence of the parameters governing the problem can be easily identified.

1.2. Contributions and structure of the paper

This paper is intended as a continuation of the work by Carbajosa et al. [13], in which a simplified, one-dimensional, quasi-stationary mathematical model, referred to as DS^2M (*Duct Shock Speed Model*), was developed. This model enables rapid estimations of the motion speed of a normal shock wave, as well as the determination of its equilibrium positions and stability. To apply the model to the hypersonic regime, the set of shock waves(known as shock-train) and subsequent subsonic compression (altogether commonly referred to as a pseudo-shock) should be replaced by an equivalent normal shock wave. The

aforementioned study also outlines how the effects of combustion can be modeled through the introduction of a second throat, provided the throat area corresponding to each value of the air-fuel ratio is known [13]. Furthermore, the DS^2M model facilitates the study of the instability known as buzz, characterized by the cyclic ingestion and expulsion of the shock wave [13].

In the work by Carbajosa et al. [13], the DS^2M model underwent extensive validation through comparisons with various experimental tests reported in the literature. Consequently, this study assumes that the validity of the DS^2M model has already been satisfactorily demonstrated. However, even if the DS^2M model is significantly simpler than other existing analytical models, it still presents certain mathematical challenges. These challenges arise not only from the need for numerical resolution but also from the difficulty in clearly estimating the influence of various parameters due to the large number of equations involved and their high degree of nonlinearity.

For this reason, the aim of the present paper is to develop various approximated methods that, albeit within a more limited range of validity, provide simplified expressions for the shock wave motion speed. These approximations allow for straightforward and reliable evaluations of the shock wave motion speed, equilibrium positions, and stability, while clearly illustrating the influence of key design parameters. Such methods are particularly useful in very early design stages, where programming a numerical solution to the DS^2M equations could not be accommodated. Additionally, the analytical expressions derived in this study offer insights into the effects of the parameters involved. From now on, the term DS^2M will refer to the model as presented by Carbajosa et al. [13], while distinct extensions (*i.e.*, DS^2M-X models) will denote the successive approximation levels introduced in this work.

This paper is organized as follows. In Section 2, the approximated formulations of the DS^2M model by Carbajosa et al. [13] are summarized, including First, Second, and High order expansions, along with different models for specific functions. In Section 3, the results are presented and analyzed, highlighting the similarities and differences between the approximated formulations and the outcomes of the DS^2M model. In Section 4, the conclusions are summarized. To improve readability, the document includes an initial annex introducing the list of symbols and nomenclature (Appendix A), as well as additional details of the calculations in three further annexes (Appendix B, Appendix C, and Appendix D).

2. Asymptotic expansions

Due to the high nonlinearity of the DS^2M model, analyzing trends in the shock wave motion speed using analytical expressions is challenging. Therefore, this paper introduces several approximations of varying degrees of accuracy and complexity, enabling results to be obtained without resorting to numerical techniques for solving the exact equations.

To this end, asymptotic expansions are applied to the general expressions provided by the DS^2M model. Therefore, in addition to the small perturbation assumptions made in the development of each of the simplified models, it is also necessary to consider the assumptions originally proposed by Carbajosa et al. [13] in the formulation of the DS^2M model. The influence of viscosity on the shock wave dynamics, which is neglected in the DS^2M model, can also be incorporated to predict more realistic solutions. Section 3.1 provides a qualitative discussion of the influence of fluid viscosity on the shock wave dynamics.

As outlined in the work by Carbajosa et al. [13], when seeking to determine the motion speed of a normal shock wave within a duct as a function of its position along the duct (see Fig. 2 and Appendix A for the nomenclature), it is useful to distinguish between the N reference frame, fixed to the duct, and the W reference frame, fixed to the shock wave. Additionally, the Mach number at the inlet, M^P_{N1}, and the stagnation temperature at the inlet, T^P_{Ns}, in the N reference frame are assumed to be known, which is equivalent to fixing a flight

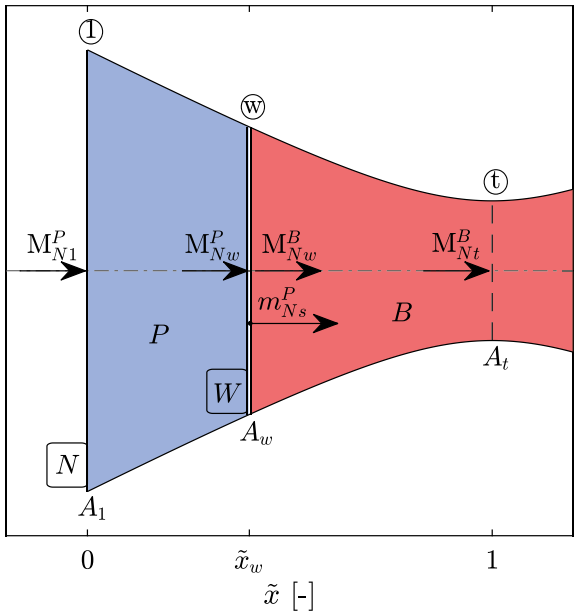

Fig. 2. Sketch of the inlet considered. The throat, A_t, is assumed to be at critical conditions. P and B: supersonic (blue region) and subsonic (red region) branches, respectively. Symbols defined in Appendix A. (For interpretation of the references to color in this figure legend, the reader is referred to the web version of this article.)
Source: Adapted from [13].

condition determined by a given Mach number and height above the ground. Similarly, the duct area distribution (which is assumed to be smooth enough as to consider the flow one-dimensional), $A(x)$, as a function of the longitudinal coordinate measured from the inlet lip, x, is also considered known. This area distribution can be expressed in dimensionless form as:

$$\eta(\tilde{x}) = A(\tilde{x})/A_1 \leq 1, \quad \text{being} \quad \tilde{x} = x/L, \tag{1}$$

where A_1 represents the inlet area, $\tilde{x} = x/L$ is the dimensionless longitudinal position, and L is the longitudinal distance between the inlet and the throat. The dimensionless areas of the throat and shock wave sections are given as:

$$\eta_t = A_t/A_1 \quad \text{and} \quad \eta_w = A_w/A_1, \tag{2}$$

respectively. The relevant quantities are generally evaluated at three locations: the inlet ($_1$), the throat ($_t$), and the shock wave position ($_w$). Additionally, these quantities may refer to the supersonic branch (^{P}) or the subsonic branch (^{B}), or they may be defined in a reference frame fixed to the inlet ($_N$) or to the shock wave ($_W$). Some quantities, such as stagnation or total values ($_s$), depend on the reference frame in which they are expressed. For reference-independent quantities, such as static temperature, no subscript is used.

The expansion of the approximated formulations is based on asymptotic methods for Mach numbers close to 1, and for ducts with section area values close to the inlet area, A_1, or the throat area, A_t. For this purpose, the Mach numbers are expressed as:

$$\mathrm{M} = 1 + \varepsilon \quad \text{where} \quad |\varepsilon| \ll 1, \tag{3}$$

and the area ratios as:

$$\eta(\tilde{x}) = A(\tilde{x})/A_1 \quad \text{and} \quad \delta(\tilde{x}) = A(\tilde{x})/A_1 - 1 = \eta(\tilde{x}) - 1. \tag{4}$$

In particular, $\delta_1 = \delta(\tilde{x} = 0) = 0$, $\delta_t = \eta_t - 1$, and $\delta_w = \eta_w - 1$. The ratio of the area of a given section to the critical section (which varies from one branch, P or B, to the other) is expressed in the form $a(\mathrm{M}) = A(\mathrm{M})/A^* - 1$. It is assumed that the terms $|\delta(\tilde{x})| \ll 1$ and $|a(\mathrm{M})| \ll 1$ are small compared to unity, regardless of the section or

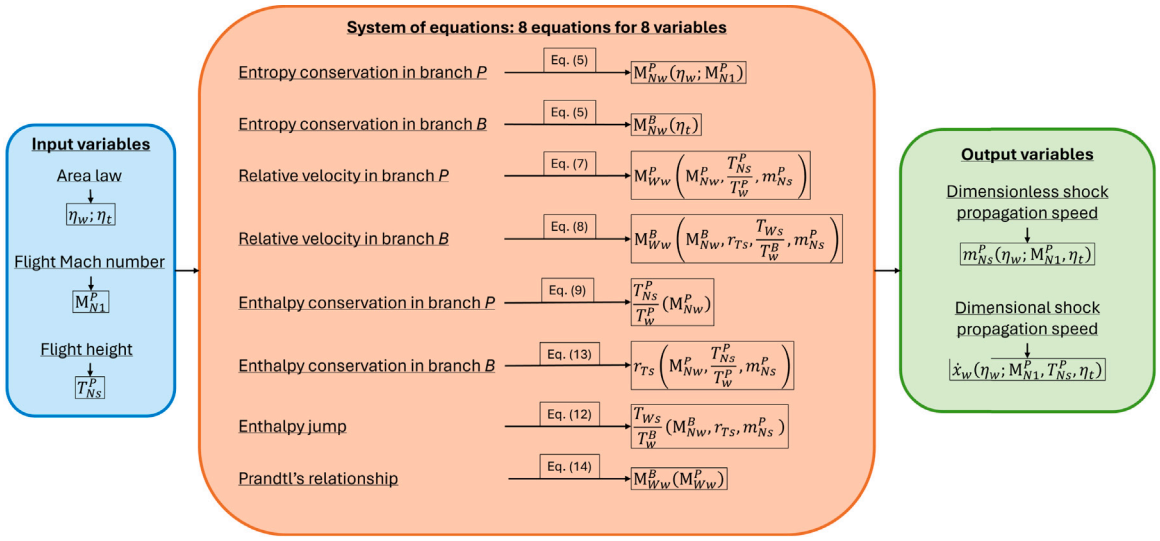

Fig. 3. Flowchart of the DS^2M model developed by Carbajosa et al. [13]. Input variables are depicted in blue, whereas intermediate equations are colored in orange and the main output variables appear in green. Symbols defined in Appendix A. (For interpretation of the references to color in this figure legend, the reader is referred to the web version of this article.)

reference frame considered. Additionally, the specific heat ratio of air is taken as $\gamma = 1.4$. Where appropriate, general expressions as functions of γ are also provided.

2.1. General expressions

Before dealing with the approximated formulations, it is appropriate, for clarity, to recall some expressions derived from the DS^2M model proposed by Carbajosa et al. [13], which will be referenced throughout this text. Fig. 3 shows the flowchart followed by the DS^2M model.

For the upstream and downstream flow of the shock wave, assuming a one-dimensional, steady, and isentropic flow in a duct, the relationship between the area at each section, A, and the Mach number in that section, M, is given by [4]:

$$\frac{A(\mathrm{M})}{A^*} = \frac{1}{\mathrm{M}}\left[\frac{2}{\gamma+1}\left(1+\frac{\gamma-1}{2}\mathrm{M}^2\right)\right]^{\frac{\gamma+1}{2(\gamma-1)}}, \tag{5}$$

where A^* is the critical area, and γ is the ratio of specific heats for air. In the above expression two branches can be considered (see Fig. 1): B for subsonic Mach numbers ($\mathrm{M} \leq 1$) and P for supersonic Mach numbers ($\mathrm{M} \geq 1$). The critical area differs upstream and downstream of the shock wave due to the dissipation in the shock wave, which is associated with a change in the stagnation pressure. Specifically, upstream of the shock wave (supersonic flow) is $A^* \equiv A^{P*} = A^*_1$, while downstream of the shock wave (subsonic flow) is $A^* \equiv A^{B*} = A_t$.

Regarding the motion of the shock wave within the duct, the conditions on both sides of the shock wave—upstream and downstream—must satisfy the Prandtl relationship between the Mach number of the flow incident on the shock wave, M_i, and the Mach number of the flow exiting the shock wave, M_d, in the shock wave reference frame, W:

$$\mathrm{M}_d(\mathrm{M}_i) = \sqrt{\frac{1+\frac{\gamma-1}{2}\mathrm{M}_i^2}{\gamma\mathrm{M}_i^2-\frac{\gamma-1}{2}}}, \quad \text{with} \quad \mathrm{M}_i \geq 1. \tag{6}$$

The relationships between the Mach numbers for the supersonic and subsonic branches in coordinates fixed to the duct (M^P_{Nw} and M^B_{Nw}) and in reference frames fixed to the shock wave (M^P_{Ww} and M^B_{Ww}), respectively, are expressed as:

$$\mathrm{M}^P_{Ww} = \mathrm{M}^P_{Nw} - \frac{\dot{x}_w}{\sqrt{\gamma R_g T^P_w}} \Rightarrow \mathrm{M}^P_{Ww} = \mathrm{M}^P_{Nw} - \sqrt{\frac{T^P_{Ns}}{T^P_w}}m^P_{Ns}, \quad \text{and} \tag{7}$$

$$\mathrm{M}^B_{Ww} = \mathrm{M}^B_{Nw} - \frac{\dot{x}_w}{\sqrt{\gamma R_g T^B_w}} \Rightarrow \mathrm{M}^B_{Ww} = \mathrm{M}^B_{Nw} - \sqrt{r_{Ts}}\sqrt{\frac{T_{Ws}}{T^B_w}}m^P_{Ns}, \tag{8}$$

in terms of the stagnation temperature ratio, $r_{Ts} = T^P_{Ns}/T_{Ws}$, and the dimensionless shock wave motion speed (assumed positive from the inlet entrance towards the throat), $m^P_{Ns} = \dot{x}_w/\sqrt{\gamma R_g T^P_{Ns}}$. The relationship between the stagnation temperature upstream of the shock wave, T^P_{Ns}, and the static temperature immediately upstream of the shock wave, T^P_w, is given by:

$$\frac{T^P_{Ns}}{T^P_w} = 1+\frac{\gamma-1}{2}\left(\mathrm{M}^P_{Nw}\right)^2, \tag{9}$$

where the Mach number at this position, M^P_{Nw}, is given in an implicit form by:

$$\frac{A(\mathrm{M}^P_{Nw})}{A^{P*}} = \frac{A_1}{A^*_1}\eta_w \tag{10}$$

as a function of $\eta_w = \eta(\bar{x}_w)$ and M^P_{N1}.

Likewise, the ratio of the stagnation temperature in the shock wave's reference frame, T_{Ws}, to the static temperature in the supersonic branch at the shock wave position, T^P_w, is given by:

$$\frac{T_{Ws}}{T^P_w} = 1+\frac{\gamma-1}{2}\left(\mathrm{M}^P_{Ww}\right)^2 = 1+\frac{\gamma-1}{2}\left(\mathrm{M}^P_{Nw}-\sqrt{\frac{T^P_{Ns}}{T^P_w}}m^P_{Ns}\right)^2, \tag{11}$$

where M^P_{Ww} is derived from Eq. (7). Dividing Eq. (9) by Eq. (11), one obtains:

$$r_{Ts} \equiv \frac{T^P_{Ns}}{T_{Ws}} = \frac{1+\frac{\gamma-1}{2}\left(\mathrm{M}^P_{Nw}\right)^2}{1+\frac{\gamma-1}{2}\left(\mathrm{M}^P_{Nw}-\sqrt{\frac{T^P_{Ns}}{T^P_w}}m^P_{Ns}\right)^2}. \tag{12}$$

According to the expression given by Carbajosa et al. [13], the ratio of the stagnation temperature in the shock wave's reference frame, T_{Ws}, to the static temperature in the subsonic branch at the shock wave position, T^B_w, is expressed as:

$$\sqrt{\frac{T_{Ws}}{T^B_w}} = \frac{(\gamma-1)\sqrt{r_{Ts}}m^P_{Ns}}{2\left(1-\frac{\gamma-1}{2}r_{Ts}m^P_{Ns}\right)}$$

$$\times \left(-1 \pm \sqrt{1 + 4 \frac{\left(1 - \frac{\gamma-1}{2} r_{Ts} m_{Ns}^P\right)\left(1 + \frac{\gamma-1}{2}\left[\mathrm{M}_{Nw}^B\right]^2\right)}{\left((\gamma-1)\sqrt{r_{Ts}} m_{Ns}^P\right)^2}} \right), \quad (13)$$

Using Eqs. (12) and (13), the Mach numbers for both the subsonic and supersonic flows relative to the shock wave (M_{Ww}^B and M_{Ww}^P), can be determined using Eqs. (7) and (8), respectively, in terms of the four variables $(\eta_w, m_{Ns}^P; \mathrm{M}_{N1}^P, \eta_t)$. Consequently, imposing the Prandtl relation given by Eq. (6), the following implicit equation is obtained to derive $m_{Ns}^P = m_{Ns}^P(\eta_w; \mathrm{M}_{N1}^P, \eta_t)$:

$$\mathrm{M}_{Ww}^B = \sqrt{\frac{1 + \frac{\gamma-1}{2}\left(\mathrm{M}_{Ww}^P\right)^2}{\gamma\left(\mathrm{M}_{Ww}^P\right)^2 - \frac{\gamma-1}{2}}}. \quad (14)$$

In what follows, the method of the asymptotic expansions of increasing order will be used to simplify the relationships presented thus far, in terms of ε powers, where $\varepsilon = \mathrm{M} - 1$.

2.2. First order expansion

First, an approximated formulation is developed, leading to the so-called $DS^2M - F$ model (*Duct Shock Speed Model-First order expansion*), where Taylor expansions of the DS^2M formulation are performed, retaining only the first term in each expansion. The variation of the area with the Mach number given by Eq. (5) for $|\mathrm{M} - 1| \ll 1$ can be expressed in a linearized form as:

$$a(\varepsilon) = \frac{A(\mathrm{M})}{A^*} - 1 \approx k_{A2}\varepsilon^2, \quad (15)$$

where $\varepsilon = \mathrm{M} - 1$, and $k_{A2} = 2/(\gamma+1) = 5/6$ (for $\gamma = 1.4$). This facilitates the calculation of the area A as a function of the Mach number, M, in the vicinity of $\mathrm{M} = 1$ along the duct. Furthermore, the Prandtl relation given by Eq. (6) can be expanded in a series assuming $\mathrm{M}_i = 1 + \varepsilon_i$, yielding, upon retaining only the first term in ε_i of the expansion:

$$\begin{aligned} \mathrm{M}_i &= 1 + \varepsilon_i \\ \mathrm{M}_d(\varepsilon_i) &\approx 1 - \varepsilon_i. \end{aligned} \quad (16)$$

To determine the value of the critical area in the supersonic branch, A^{P*}, for a given inlet entrance area, A_1, Eq. (15) is first evaluated at the inlet entrance, where the Mach number in the reference frame fixed to the inlet is known:

$$a_1 = \frac{A_1}{A^{P*}} - 1 \approx k_{A2}\left(\varepsilon_{N1}^P\right)^2. \quad (17)$$

Likewise, using Eq. (15), the Eq. (5) for the Mach number at the shock wave position in the inlet reference frame, N, $\mathrm{M}_{Nw}^P = 1 + \varepsilon_{Nw}^P$, in the supersonic branch P, takes the form:

$$\frac{A_w}{A^{P*}} = \left(1 + a_1\right)\eta_w = 1 + a_w^P \approx 1 + k_{A2}(\varepsilon_{Nw}^P)^2, \quad (18)$$

where rearranging terms and solving for ε_{Nw}^P yields:

$$\begin{aligned} \varepsilon_{Nw}^P &\approx +\sqrt{\frac{a_w^P}{k_{A2}}} = +\sqrt{\frac{\delta_w + a_1\eta_w}{k_{A2}}} = \frac{1}{\sqrt{k_{A2}}}\sqrt{\frac{A_w\left(1 + a_1\right)}{A_1} - 1} \\ &= \frac{1}{\sqrt{k_{A2}}}\sqrt{\frac{A_w}{A_1}\left[1 + k_{A2}(\varepsilon_{N1}^P)^2\right] - 1}. \end{aligned} \quad (19)$$

The + sign is chosen because ε^P corresponds to the supersonic branch. The Mach number relative to unity, ε_{Nw}^P, depends on the area at the wave position A_w/A_1 and the inlet Mach number ε_{N1}^P. Similarly, in the subsonic region immediately behind the shock wave:

$$\frac{A_w}{A^{B*}} = \frac{\eta_w}{\eta_t} = 1 + a_w^B \approx 1 + k_{A2}(\varepsilon_{Nw}^B)^2, \quad (20)$$

leading to:

$$\varepsilon_{Nw}^B \approx -\sqrt{\frac{a_w^B}{k_{A2}}} = -\sqrt{\frac{\delta_w - \delta_t}{k_{A2}\eta_t}} = -\frac{1}{\sqrt{k_{A2}}}\sqrt{\frac{A_w}{A_t} - 1}. \quad (21)$$

The − sign is chosen because ε^B corresponds to the subsonic branch. The Mach number relative to unity, ε_{Nw}^B, depends only on the area A_w/A_t.

The incident Mach number at the shock wave in the shock wave reference frame is $\mathrm{M}_i \equiv \mathrm{M}_{Ww}^P$, while the outgoing Mach number is $\mathrm{M}_d \equiv \mathrm{M}_{Ww}^B$. By adding both terms using the approximated expression of the Prandtl relation given by Eq. (16), ε_i is eliminated, yielding:

$$\mathrm{M}_i + \mathrm{M}_d \equiv \mathrm{M}_{Ww}^P + \mathrm{M}_{Ww}^B \approx 2. \quad (22)$$

By substituting the values of M_{Ww}^P and M_{Ww}^B from the exact Eqs. (7) and (8) into Eq. (22), we obtain:

$$\mathrm{M}_{Ww}^P + \mathrm{M}_{Ww}^B = \mathrm{M}_{Nw}^P - \sqrt{\frac{T_{Ns}^P}{T_w^P}} m_{Ns}^P + \mathrm{M}_{Nw}^B - \sqrt{r_{Ts}}\sqrt{\frac{T_{Ws}}{T_w^B}} m_{Ns}^P \approx 2, \quad (23)$$

which, expressing the Mach numbers in terms of ε_{Nw}^P and ε_{Nw}^B, results in:

$$\mathrm{M}_{Ww}^P + \mathrm{M}_{Ww}^B \approx \left(1 + \varepsilon_{Nw}^P\right) + \left(1 + \varepsilon_{Nw}^B\right) - m_{Ns}^P\left[\sqrt{\frac{T_{Ns}^P}{T_w^P}} + \sqrt{r_{Ts}}\sqrt{\frac{T_{Ws}}{T_w^B}}\right] \approx 2, \quad (24)$$

from which:

$$m_{Ns}^P\left[\sqrt{\frac{T_{Ns}^P}{T_w^P}} + \sqrt{r_{Ts}}\sqrt{\frac{T_{Ws}}{T_w^B}}\right] \approx \varepsilon_{Nw}^P + \varepsilon_{Nw}^B. \quad (25)$$

In this limit, where $|\varepsilon_{Nw}^P|, |\varepsilon_{Nw}^B| \ll 1$, the motion speed of the shock wave itself satisfies $|m_{Ns}^P| \ll 1$. Therefore, only terms of unit order are retained in the parentheses multiplying m_{Ns}^P. Using the exact expressions (see Eqs. (9), (12) and (13) in Carbajosa et al. [13]), and retaining unit-order terms, the following approximated expressions are obtained (as though the local temperatures were critical temperatures, and the stagnation temperature is conserved in both reference frames N and W):

$$\frac{T_{Ns}^P}{T_w^P} \approx \frac{T_{Ws}}{T_w^B} \approx \frac{\gamma+1}{2} \Rightarrow r_{Ts} \approx 1. \quad (26)$$

Thus, the shock wave motion speed can be directly obtained from Eq. (25) as:

$$m_{Ns}^P|_F \approx C_1^F\left[\varepsilon_{Nw}^P + \varepsilon_{Nw}^B\right], \quad (27)$$

where $C_1^F = 1/\sqrt{2(\gamma+1)} \simeq 0.456$ (for $\gamma = 1.4$). Using Eqs. (19) and (21), and noting that $C_1^F/\sqrt{k_{A2}} = 1/2$, Eq. (25) becomes:

$$m_{Ns}^P|_F \approx \frac{1}{2}\left(\sqrt{a_w^P} - \sqrt{a_w^B}\right), \quad (28)$$

which provides the dimensionless motion speed of the shock wave as a function of a_w^P and a_w^B, which are the dimensionless areas at the shock wave position, referenced to the critical areas before (P) and after (B) the shock wave, respectively. In the above expression, a_w^P is obtained from Eqs. (17) and (18):

$$a_w^P = \left[1 + k_{A2}\left(\varepsilon_{N1}^P\right)^2\right]\eta_w - 1, \quad (29)$$

and a_w^B from Eq. (20):

$$a_w^B = \frac{\eta_w}{\eta_t} - 1. \quad (30)$$

Substituting Eqs. (29) and (30) into Eq. (28), the result is:

$$m_{Ns}^P|_F \approx \frac{1}{2}\left(\sqrt{\left[1 + k_{A2}\left(\varepsilon_{N1}^P\right)^2\right]\eta_w - 1} - \sqrt{\frac{\eta_w}{\eta_t} - 1}\right). \quad (31)$$

Therefore, the dimensionless motion speed depends on the shock wave section area, η_w, the throat area, η_t, and the inlet Mach number, ε_{N1}^P. The equilibrium position of the shock wave, $\eta_w^z|_F$, where the shock

wave motion speed vanishes, is found by setting the previous expression to zero:

$$\eta_t^z|_F = \frac{1}{1+k_{A2}\left(\varepsilon_{N1}^P\right)^2} \approx 1 - k_{A2}\left(\varepsilon_{N1}^P\right)^2, \tag{32}$$

yielding the expression for the IS and KD limits, which coincide in the DS^2M-F model.

The maximum and minimum shock wave motion speeds allow for the identification of the regions where the shock wave travels at higher speeds. They also serve to evaluate the validity of the approximations made, given that the motion speed has been assumed to be low enough (much lower than the speed of sound). This assumption has enabled a further simplification of the original DS^2M model, in which it was already considered that the motion speed was small enough to neglect highly unsteady effects, such as those associated with acoustic waves. Given the interest in determining such extreme motion speeds, in order to find the maximum or minimum shock wave motion speed according to the DS^2M-F model, from Eq. (31):

$$\frac{\mathrm{d}m_{Ns}^P|_F}{\mathrm{d}\tilde{x}_w} = \frac{\mathrm{d}m_{Ns}^P|_F}{\mathrm{d}\eta_w}\frac{\mathrm{d}\eta_w}{\mathrm{d}\tilde{x}_w} = 0. \tag{33}$$

From Eq. (33), there are two possibilities: $\mathrm{d}\eta_w/\mathrm{d}\tilde{x}_w = 0$ or $\mathrm{d}m_{Ns}^P|_F/\mathrm{d}\eta_w = 0$. In the first case, the maximum motion speed occurs at the throat, and at other places where the duct area law has zero derivative. In the second case, from Eq. (31):

$$\frac{\mathrm{d}m_{Ns}^P|_F}{\mathrm{d}\eta_w} = \frac{1+k_{A2}\left(\varepsilon_{N1}^P\right)^2}{4\sqrt{\left[1+k_{A2}\left(\varepsilon_{N1}^P\right)^2\right]\eta_w^m|_F - 1}} - \frac{1/\eta_t}{4\sqrt{\frac{\eta_w^m|_F}{\eta_t}-1}} = 0, \tag{34}$$

from which the dimensionless area at the shock wave position, $\eta_w^m|_F$, where the extreme value of $m_{Ns}^P|_F$ is reached, is determined as:

$$\eta_w^m|_F = \eta_t \frac{1-1/\left[\eta_t\left(1+k_{A2}\left(\varepsilon_{N1}^P\right)^2\right)\right]^2}{1-1/\left[\eta_t\left(1+k_{A2}\left(\varepsilon_{N1}^P\right)^2\right)\right]} = \eta_t\left(1+\frac{1}{k_{A2}\left(\varepsilon_{N1}^P\right)^2}\right) \gg \eta_t. \tag{35}$$

Since $\varepsilon_{N1}^P \ll 1$, the extreme value of $m_{Ns}^P|_F$ is reached at $\eta_w^m|_F \gg \eta_w \sim \eta_t$, which falls outside the range of validity of this model. Since the shock wave motion speed is monotonically increasing or decreasing (within the DS^2M-F model), and it is assumed that $\eta_w \geq \eta_t$, the maximum or minimum shock wave motion speed conditions are reached at the throat.

Once the dimensionless motion speed of the shock wave is obtained from Eq. (31), the dimensional speed, acceleration, and trajectory of the shock wave can be obtained from Appendix C in Carbajosa et al. [13].

To analyze the motion speed as a function of position, it is useful to rewrite Eq. (28) as:

$$m_{Ns}^P|_F = \frac{1}{2}\frac{a_w^P - a_w^B}{\sqrt{a_w^P}+\sqrt{a_w^B}}, \tag{36}$$

and express a_w^P in terms of the area jump across the wave, ξ, defined as:

$$\xi = a_w^P - a_w^B = \frac{A_w}{A_t}\left(\frac{A_t}{A^{P*}}-1\right) \approx \eta_w\left(\frac{\eta_t-1}{\eta_t}+k_{A2}\left(\varepsilon_{N1}^P\right)^2\right)$$
$$= \frac{A_w}{A_1}\left(1-\frac{A_1}{A_t}+k_{A2}\left(\varepsilon_{N1}^P\right)^2\right). \tag{37}$$

Note that the case $\xi = 0$ ($a_w^P = a_w^B$) corresponds to both the IS and KD curves, as well as the zero-speed curve within this first approximation, as shown below.

Thus, if the inlet geometry variations are smooth, and the difference between the entrance and throat areas is small, when the shock wave section area and inlet Mach number ε_{N1}^P satisfy $|\xi| \ll a_w^B, a_w^P$, the shock wave motion speed can be approximated as:

$$m_{Ns}^P|_{F,\,\xi\ll1} \approx \frac{1}{4}\frac{\xi}{\sqrt{\frac{\eta_w}{\eta_t}-1}} = \frac{1}{4}\frac{\xi}{\sqrt{\frac{A_w}{A_t}-1}} = \frac{1}{4}\frac{A_w/A_t}{\sqrt{\frac{A_w}{A_t}-1}}\left(\frac{A_t}{A^{P*}}-1\right), \tag{38}$$

where the condition $A_w > A_t$ is always fulfilled if the shock is not at the throat. The motion speed of the shock wave has the same sign as the area jump ξ, or $\left(A_t - A^{P*}\right)$.

If the shock wave is placed at an area $A_w \approx A_1$, the limit $\eta_w \to 1$ can be considered. Using the approximation $A_1/A^{P*} \approx 1 + k_{A2}\left(\varepsilon_{N1}^P\right)^2$, it follows that:

$$m_{Ns}^P|_{F,\,\xi\ll1,\,A_1} \approx \frac{1}{4}\frac{\frac{A_1}{A_t}}{\sqrt{\frac{A_1}{A_t}-1}}\left(\frac{A_t}{A^{P*}}-1\right). \tag{39}$$

For a large throat area, $A_t > A^{P*}$ (*i.e.*, $\xi > 0$), the dimensionless motion speed is $m_{Ns}^P|_{F,\,\xi\ll1,\,A_1} > 0$ (the shock wave is swallowed). If $A_t = A^{P*}$, then $m_{Ns}^P|_{F,\,\xi\ll1,\,A_1} = 0\ \forall A_w$, but this result is not valid, it is a consequence of the first-order approximation. For a better precision, higher-order terms should be retained. Here, $A_t = A^{P*}$ corresponds to the $IS \equiv KD$ curve, and the configuration is at the stability limit. In this approximation, shock waves whose configurations are placed on these curves are not moving.

The isentropic curve IS is obtained from Eq. (21), which leads to $\varepsilon_{Nw}^B = 0$ as the shock wave is at the throat ($x_w = x_t$, $A_w = A_t \equiv A^{P*}$). Thus, from Eq. (15), it follows:

$$\left(A_1/A_t\right)_{IS} = 1 + k_{A2}\left(\varepsilon_{N1}^P\right)^2. \tag{40}$$

This expression can also be obtained by considering the supersonic isentropic evolution up to the throat, where $A_t = A^{P*}$ and the Mach number at the throat is unity ($\varepsilon_{Nw}^P \equiv \varepsilon_{Nt}^P = 0$). Thus, from Eq. (17), we obtain $A_t(1+a_1)/A_1 - 1 = 0$, and combining this with Eq. (15) leads to Eq. (40).

The curve corresponding to the Kantrowitz-Donaldson limit, KD, is defined by $\varepsilon_{Nw}^P \equiv \varepsilon_{N1}^P$ because the shock wave is located at the inlet entrance. From Eq. (21):

$$\varepsilon_{Nw}^B \equiv \varepsilon_{N1}^B = -\sqrt{\frac{A_1/A_t-1}{k_{A2}}}, \tag{41}$$

where $A_t = \left(A^{P*}\right)_{M_d}$. Since the Mach number jump across the shock wave is $\varepsilon_{Nw}^P \equiv \varepsilon_{N1}^P = -\varepsilon_{Nw}^B \equiv -\varepsilon_{N1}^B$ (if the shock wave is standing still), it follows from Eq. (41) that:

$$\left(A_1/A_t\right)_{KD} = 1 + k_{A2}\left(\varepsilon_{N1}^B\right)^2. \tag{42}$$

Within this first-order approximation, is $|\varepsilon_{N1}^B| = |\varepsilon_{N1}^P|$. Consequently, from Eqs. (40) and (42), both curves IS and KD coincide, and no hysteresis region appears. This occurs because the curve $A(\mathrm{M})/A^*$ is symmetric about M = 1 in this first approximation, as it depends on $(\mathrm{M}-1)^2$, and the Mach number downstream the shock wave, $|\varepsilon_{Nw}^B| = \varepsilon_{Nw}^P$, is also symmetric (see Fig. 4). To introduce an asymmetry with respect to M = 1, it would be necessary to retain higher-order terms (ε_N^3), and therefore also an asymmetry in the Mach number behind the shock wave ($1-\varepsilon_i$) compared to the Mach number ahead of it ($1+\varepsilon_i$). Therefore, with this first-order approximation, it is only possible to calculate the shock wave motion speed above the KD curve (positive speeds) or below the IS curve (negative speeds), but not in the intermediate region, which does not exist in this approximation. Indeed, as shown in Fig. 5, the IS and KD curves collapse into a single curve in this approximation.

When the shock wave is at the throat, $\eta_w = \eta_t$, Eq. (38) cannot be used, and from Eq. (30), it can be seen that $a_w^B = 0$, and the speed, in approximated terms, becomes:

$$m_{Ns}^P|_{F,\,\xi\ll1,\,A_t} \approx \frac{\sqrt{a_w^P}}{2} = \frac{\sqrt{\xi}}{2} \geq 0 \ \text{(valid if } \xi > 0). \tag{43}$$

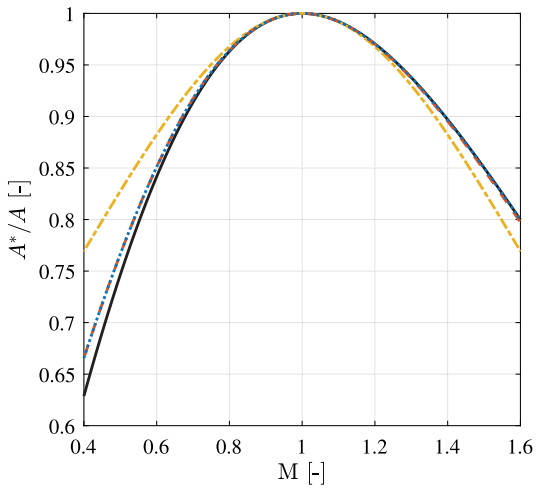

Fig. 4. Ratio of the critical area to the area at each section, A^*/A, as a function of the Mach number, M, obtained using the DS^2M model (see Eq. (5)) (solid line) and the approximated methods (see Appendix C): **Method 1** (dash-dotted line), **Method 2** (dashed line), and **Method 3** (dotted line) of the DS^2M-H model (see Appendix C).

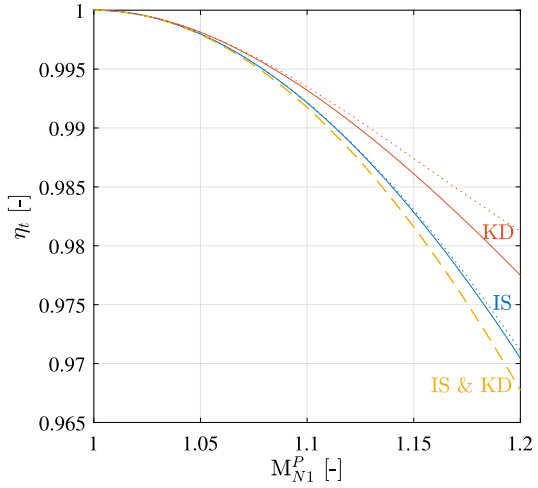

Fig. 5. IS and KD curves obtained using the DS^2M model (solid lines), the DS^2M-F model (dashed line), and the DS^2M-S model (dotted lines). In the depicted scale, DS^2M and DS^2M-H models present practically the same behavior.

If $\xi > 0$, the throat swallows the shock wave. To analyze the expelling process of the shock wave when the IS limit is reached, consider the following: if according to Eq. (43) the shock wave has zero speed when located at the throat ($\xi = 0$) with an area $A_t = A_{t0} \equiv A^{P*}$, and the throat area is abruptly reduced to $A_t = A_{tc} < A_{t0}$, then $a_w^B = A_w/A_{tc} - 1 > 0$ increases sharply (see Eqs. (29), (30) and (37)), and therefore, $\xi < 0$. Therefore, Eq. (43) cannot be applied. However, as the shock wave moves quickly upstream, $A_w > A_{t0}$ and $A_t = A_{tc} < A^{P*}$, from Eq. (38) it follows that $m^P_{Ns}|_{F,\,\xi\ll 1,\,A_1} < 0$, and therefore the shock wave moves upstream (to the left), being expelled to accommodate the excess flow that cannot pass through the throat (which corresponds to subsonic flow behind the shock wave). This occurs because the area required to block the throat for subsonic flow is significantly larger than the critical area suitable for supersonic flow.

2.3. Second order expansion

As discussed in the previous section, in the results of the first approximation (DS^2M-F model) no difference between IS and KD can be found, since it lacks asymmetry around M = 1. To refine these and other details, it is necessary to develop a more precise formulation. To achieve this, the Taylor series expansions of the DS^2M model should retain at least the first two terms, leading to the DS^2M-S model (*Duct Shock Speed Model-Second order expansion*). In this way, Eq. (5) can be approximated as:

$$a(\varepsilon) = \frac{A(\varepsilon)}{A^*} - 1 \approx k_{A2}\varepsilon^2 + k_{A3}\varepsilon^3, \tag{44}$$

where $k_{A2} = 2/(\gamma+1) = 5/6$ and $k_{A3} = -2(5\gamma-3)/(3(\gamma+1)^2) = -25/54$ (for $\gamma = 1.4$). Additionally, in the Prandtl relationship (see Eq. (6)), the consideration of the second order term in the Taylor series expansion leads to:

$$\mathrm{M}_d(\varepsilon_i) \approx 1 - \varepsilon_i + k_{\mathrm{M}2}\varepsilon_i^2 + \cdots, \tag{45}$$

where $k_{\mathrm{M}2} = (3\gamma-1)/(\gamma+1) = 4/3$ (for $\gamma = 1.4$).

Next, to obtain the supersonic Mach number in the inlet reference frame at the various sections of interest, the approximated expression for Eq. (15), evaluated at the inlet using Eq. (44), is given now as:

$$a_1 = \frac{A_1}{A_1^*} - 1 \approx k_{A2}\left(\varepsilon^P_{N1}\right)^2 + k_{A3}\left(\varepsilon^P_{N1}\right)^3. \tag{46}$$

Similarly, Eq. (15), evaluated upstream of the shock wave, takes the form:

$$\frac{A_w}{A^{P*}} \equiv \left(1+a_1\right)\eta_w = 1 + a_w^P \approx 1 + k_{A2}(\varepsilon^P_{Nw})^2 + k_{A3}(\varepsilon^P_{Nw})^3. \tag{47}$$

Likewise, Eq. (15), evaluated downstream of the shock wave, has the following approximated form:

$$\frac{A_w}{A^{B*}} \equiv \frac{\eta_w}{\eta_t} = 1 + a_w^B \approx 1 + k_{A2}(\varepsilon^B_{Nw})^2 + k_{A3}(\varepsilon^B_{Nw})^3. \tag{48}$$

It can be shown that both Eqs. (47) and (48) share the same structure, that is:

$$k_{A2}\epsilon^2 + k_{A3}\epsilon^3 \approx a. \tag{49}$$

In Appendix B, the detailed derivation of the Mach number is obtained as a function of the dimensionless area a. This derivation starts from Eq. (49), and results in:

$$\epsilon(a) \cong \pm\sqrt{a/k_{A2}} - k_{A3}a/(2k_{A2}), \tag{50}$$

where the + sign corresponds to the supersonic solution, P, and the − sign corresponds to the subsonic solution, B. The first term (which changes sign) is identical to the DS^2M-F model and represents a symmetric effect, while the second term (which does not change sign) introduces an asymmetry, thereby contributing to the separation of the IS and KD limits.

Substituting Eq. (50) into Eqs. (47) and (48), and considering that $\varepsilon^P_{Nw} \geq 0$ and $\varepsilon^B_{Nw} \leq 0$, we obtain:

$$\varepsilon^P_{Nw} \approx +\sqrt{\frac{a_w^P}{k_{A2}} - \frac{k_{A3}}{2k_{A2}^2}a_w^P}, \quad \text{and} \quad \varepsilon^B_{Nw} \approx -\sqrt{\frac{a_w^B}{k_{A2}} - \frac{k_{A3}}{2k_{A2}^2}a_w^B}. \tag{51}$$

Besides, in the shock wave reference frame, the Mach number incident on the shock wave is $\mathrm{M}_i \equiv \mathrm{M}^P_{Ww}$, while the outgoing Mach number is $\mathrm{M}_d \equiv \mathrm{M}^B_{Ww}$. Following the same procedure as in the previous section (see Section 2.2), by adding Eqs. (16) and (45) we get:

$$\mathrm{M}_i + \mathrm{M}_d \equiv \mathrm{M}^P_{Ww} + \mathrm{M}^B_{Ww} \approx 2 + k_{\mathrm{M}2}\varepsilon_i^2 = 2 + k_{\mathrm{M}2}\left(\varepsilon^P_{Nw} - \sqrt{T^P_{Ns}/T^P_w}\,m^P_{Ns}\right)^2, \tag{52}$$

where:

$$\varepsilon_i = \varepsilon^P_{Nw} - \sqrt{T^P_{Ns}/T^P_w}\,m^P_{Ns}. \tag{53}$$

Adding Eqs. (7) and (8), the following is obtained:

$$\mathrm{M}^P_{Ww} + \mathrm{M}^B_{Ww} = \mathrm{M}^P_{Nw} - \sqrt{\frac{T^P_{Ns}}{T^P_w}}\,m^P_{Ns} + \mathrm{M}^B_{Nw} - \sqrt{r_{Ts}}\sqrt{\frac{T_{Ws}}{T^B_w}}\,m^P_{Ns}, \tag{54}$$

which, substituting the Mach numbers as functions of ε^P_{Nw} and ε^B_{Nw} (see Eq. (51) applied to the shock wave), yields:

$$\mathrm{M}^P_{Ww} + \mathrm{M}^B_{Ww} \approx 2 + \varepsilon^P_{Nw} + \varepsilon^B_{Nw} - m^P_{Ns}\left[\sqrt{\frac{T^P_{Ns}}{T^P_w}} + \sqrt{r_{Ts}}\sqrt{\frac{T_{Ws}}{T^B_w}}\right]. \tag{55}$$

Establishing equality between Eqs. (52) and (55), the following is derived:

$$m^P_{Ns}\left[\sqrt{\frac{T^P_{Ns}}{T^P_w}} + \sqrt{r_{Ts}}\sqrt{\frac{T_{Ws}}{T^B_w}}\right] + k_{\mathrm{M2}}\left(\varepsilon^P_{Nw} - \sqrt{\frac{T^P_{Ns}}{T^P_w}}m^P_{Ns}\right)^2 \approx \varepsilon^P_{Nw} + \varepsilon^B_{Nw}. \tag{56}$$

Note that the new term in k_{M2} (introduced in Eq. (45)) is a correction to the first-order Mach number expansion given by Eq. (25). However, since it is squared, the solution becomes more complex. To expand Eq. (56), the parenthesis multiplying m^P_{Ns} can be approximated to the first order in ε^P_{Nw}, ε^B_{Nw}, and m^P_{Ns} based on their exact expressions in Eqs. (9), (12) and (13). For consistency, the term $\sqrt{T^P_{Ns}/T^P_w}$ given by Eq. (9) should also be approximated to the first order in ε^P_{Nw} as:

$$\sqrt{\frac{T^P_{Ns}}{T^P_w}} \approx l_{T0} + l_{T1}\varepsilon^P_{Nw}, \tag{57}$$

where

$$l_{T0} = \sqrt{\frac{\gamma+1}{2}} \simeq 1.095 \quad \text{and} \quad l_{T1} = \frac{\gamma-1}{\sqrt{2(\gamma+1)}} \simeq 0.183. \tag{58}$$

Using this expression, the remaining term multiplying m^P_{Ns} becomes:

$$\left[\sqrt{\frac{T^P_{Ns}}{T^P_w}} + \sqrt{r_{Ts}}\sqrt{\frac{T_{Ws}}{T^B_w}}\right] \approx k_{T0} + k_{T\varepsilon^P_{Nw}}\varepsilon^P_{Nw} + k_{T\varepsilon^B_{Nw}}\varepsilon^B_{Nw} + k_{Tm}m^P_{Ns}, \tag{59}$$

where the coefficients are:

$$\begin{aligned}
k_{T0} &= \sqrt{\frac{\gamma+1}{2}} + \sqrt[4]{\frac{\gamma+1}{2}} \simeq 2.142,\\
k_{T\varepsilon^P_{Nw}} &= \frac{\gamma-1}{2}\left[\sqrt{\frac{2}{\gamma+1}} + \sqrt[4]{\frac{2^3}{(\gamma+1)^3}}\right] \simeq 0.357,\\
k_{T\varepsilon^B_{Nw}} &= -\frac{\gamma-1}{2}\frac{1}{\sqrt[4]{2(\gamma+1)^3}} \simeq -0.087, \quad k_{Tm} = \frac{\gamma-1}{2}\frac{1}{\sqrt[4]{2^3(\gamma+1)}} \simeq 0.096.
\end{aligned} \tag{60}$$

Considering the above approximations, Eq. (56) takes the form:

$$A_m\left(m^P_{Ns}\right)^2 + B_m m^P_{Ns} + C_m \approx 0, \tag{61}$$

where

$$\begin{aligned}
A_m &= k_{Tm} + k_{\mathrm{M2}}l^2_{T0},\\
B_m &= l_{T0} + \left(k_{T\varepsilon^P_{Nw}} - 2k_{\mathrm{M2}}l_{T0}\right)\varepsilon^P_{Nw} + k_{T\varepsilon^B_{Nw}}\varepsilon^B_{Nw},\\
C_m &= k_{\mathrm{M2}}\left(\varepsilon^P_{Nw}\right)^2 - \varepsilon^P_{Nw} - \varepsilon^B_{Nw}.
\end{aligned} \tag{62}$$

In Eq. (62), k_{M2} introduces the effect of the second term of the expansion of the shock outgoing flow Mach number, while k_{A3} (within ε^R_{Nw}, where $R = P$ or B, depending on the branch) introduces a third order effect in the expansion of the area as a function of the Mach number. The IS and KD curves are of zero motion speed, and are obtained from Eq. (61) with $C_m = 0$. Note that the last two terms of C_m when set to zero represent the condition for the IS and KD limits as obtained from the $DS^2M - F$ model (see Eq. (27)). The solution to Eq. (61) can be approximated as:

$$\begin{aligned}
m^P_{Ns}|_S = \frac{-B_m + \sqrt{B^2_m - 4A_mC_m}}{2A_m} &\approx C^S_1\left[\varepsilon^P_{Nw} + \varepsilon^B_{Nw}\right] + C^S_2\varepsilon^P_{Nw}\varepsilon^B_{Nw}\\
&+ C^S_3\left(\varepsilon^P_{Nw}\right)^2 + C^S_4\left(\varepsilon^B_{Nw}\right)^2,
\end{aligned} \tag{63}$$

where

$$C^S_1 \simeq +0.467,\ C^S_2 \simeq +0.233,\ C^S_3 \simeq -0.154,\ C^S_4 \simeq -0.236. \tag{64}$$

The polynomial on the right-hand side of Eq. (63) represents the second-order expansion of the central term in Eq. (63). Of the two possible solutions of Eq. (61), the one considered here in Eq. (63) is the + sign. With this choice, the selected branch is the one yielding zero wave motion speed, $m^P_{Ns}|_S = 0$, when $C_m = 0$, that is, when the Mach numbers upstream and downstream are unity ($\varepsilon^P_{Nw} = \varepsilon^B_{Nw} = 0$).

In Fig. 5, it is shown that, unlike the absence of a hysteresis region in the $DS^2M - F$ model, the inclusion of additional terms in the $DS^2M - S$ model recovers the presence of distinct IS and KD curves, as in the DS^2M model, and consequently the hysteresis zone located between the two curves. Furthermore, as the Mach number grows from unity, the agreement between the IS and KD curves of the DS^2M and $DS^2M - S$ models begins to show discrepancies amounting to a few thousandths in the range considered. The agreement between the various IS curves remains better than among the KD curves, where larger differences emerge.

2.4. High order expansion

Although the two approximated formulations presented ($DS^2M - F$ and $DS^2M - S$) allow for estimating the shock wave behavior for inlet Mach numbers very close to unity ($\mathrm{M}^P_{N1} = 1 + \varepsilon^P_{N1}$ with $\varepsilon^P_{N1} \ll 1$), they produce results that deviate significantly from those provided by the DS^2M model for Mach numbers further from unity (as previously observed in Fig. 5 and as it will be further discussed in Section 3). This problem suggested developing a simplified formulation that, while presenting clear analytic expressions, remains valid across a broader range of Mach numbers incident to the normal shock wave.

Considering the large influence of the accuracy in the approximation of the $\mathrm{M}(A/A^*)$ and $\mathrm{M}_d(\mathrm{M}_i)$ curves in the results for IS and KD limits and, therefore, in the shock wave motion speed, a new formulation is proposed that improves upon the second approximation, resulting in the so-called $DS^2M - H$ model (*Duct Shock Speed Model-High order expansion*). Instead of using a constant value for k_{A2}, higher-order Mach number expansions are introduced, specific to each chosen branch (subsonic or supersonic), to better approximate the curve $A(\mathrm{M})/A^*$. Detailed descriptions of the three proposed methods to improve the approximation of k_{A2} in each branch within the DS^2M-H model are provided in Appendix C. Similarly, Appendix D outlines the procedure used to derive the asymptotic expansion of the dimensionless motion speed as a function of the Mach number:

$$\begin{aligned}
\varepsilon^P_{Nw} &\approx +\sqrt{\frac{a^P_w}{k^P_{A2}(\varepsilon^P_{N1})}} = +\sqrt{\frac{\delta_w + a_1\eta_w}{k^P_{A2}(\varepsilon^P_{N1})}} \quad \text{and}\\
\varepsilon^B_{Nw} &\approx -\sqrt{\frac{a^B_w}{k^B_{A2}(\varepsilon^P_{N1})}} = -\sqrt{\frac{\delta_w - \delta_t}{k^B_{A2}(\varepsilon^P_{N1})\eta_t}},
\end{aligned} \tag{65}$$

yielding:

$$\begin{aligned}
m^P_{Ns}|_H(\varepsilon^P_{Nw}, \varepsilon^B_{Nw}) \approx C^H_1\left[\varepsilon^P_{Nw} + \varepsilon^B_{Nw}\right] + C^H_2\varepsilon^P_{Nw}\varepsilon^B_{Nw}\\
+ C^H_3\left[\left(\varepsilon^P_{Nw}\right)^2 + \left(\varepsilon^B_{Nw}\right)^2\right],
\end{aligned} \tag{66}$$

where $\varepsilon^P_{Nw} = \varepsilon^P_{Nw}(\tilde{x}_w; \varepsilon^P_{N1})$ and $\varepsilon^B_{Nw} = \varepsilon^B_{Nw}(\tilde{x}_w; \varepsilon^P_{N1})$ are given by Eq. (65). In Eq. (66), the coefficients take the values:

$$C^H_1 \simeq +0.456,\ C^H_2 \simeq +0.228,\ C^H_3 \simeq -0.190 \tag{67}$$

Note that the coefficient corresponding to the first two terms, C^H_1, is identical to that obtained in Eq. (27) of the DS^2M-F model (*i.e.*, $C^H_1 \equiv C^F_1$) as can be expected. Furthermore, the coefficients multiplying ε^P_{Nw} and ε^B_{Nw} are identical for all non-crossed terms. This symmetry arises because the asymmetry is directly incorporated within the definitions of k_{A2} for each method described in Appendix C, as well as within the definitions of ε^P_{Nw} and ε^B_{Nw}.

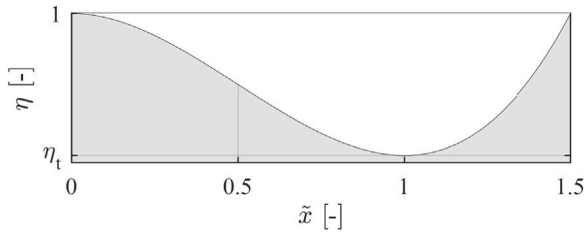

Fig. 6. Sample inlet duct area law (gray region) considered.
Source: Adapted from [13].

The results for the section area ratio to the critical area, A/A^*, as a function of Mach number M, obtained from the exact Eq. (5) and the approximated Eq. (65) for the three methods discussed in Appendix C, are presented in Fig. 4. It is shown that the best performance is achieved using **Method 3** of the DS^2M-H model, followed by **Method 2**. This is because **Method 1** is a symmetric parabola, while successive improvements introduce a $\left(\epsilon^P_{N1}\right)^3$ term that forces an enhanced antisymmetric component, bringing the approximated solutions closer to the exact curve. Henceforth, whenever the DS^2M-H model is referenced, the expressions corresponding to **Method 3** will be employed:

$$k^B_{A2}(\epsilon^P_{N1}) = k^{B3}_{A2}(\epsilon^P_{N1}),$$
$$k^P_{A2}(\epsilon^P_{N1}) = k^{P3}_{A2}(\epsilon^P_{N1}). \tag{68}$$

3. Results and discussion

Having introduced the approximated models, their results are compared to those of the DS^2M model to evaluate the validity range of each approximation. For this purpose, a sample area law is employed, given by the equation (see Fig. 6):

$$\eta(\tilde{x}) = A(\tilde{x})/A_1 = 1 + 6\zeta\left(\frac{\tilde{x}^3}{3} - \frac{\tilde{x}^2}{2}\right), \tag{69}$$

where $\zeta = 1-\eta_t$ is the throat deformation. This area law was chosen due to its simple form, and because it exhibits a null derivative at both the inlet entrance ($\tilde{x}=0$) and the throat ($\tilde{x}=1$). The interest in choosing an area law with null derivatives at the inlet entrance and throat relies on the fact that there will not be abrupt changes in the shock wave motion speed in those sections, which are the two most important sections in the inlet in terms of overall stability.

The five cases selected for the comparison are shown in Fig. 7: $M^P_{N1}=1.01$ (Fig. 8-(a)), 1.10 (Fig. 8-(b)), 1.20 (Fig. 8-(c)), 1.50 (Fig. 9-(a)), and 1.80 (Fig. 9-(b)). For each Mach number, five throat areas were considered, whose values are given in Table 1. For each point in Fig. 7, the dimensionless shock wave motion speed, m^P_{Ns}, is obtained as a function of the dimensionless position along the duct, $\tilde{x}_w$, using the proposed models. The results are normalized to $m^P_{Ns}|_{max}$, the maximum value within the interval $0<\tilde{x}_w<1$ obtained using the DS^2M model. As the results for the points placed on the IS and KD limits ($P2$ and $P4$) are very sensitive to the value assumed for these limits, to be consistent, the values used for the IS and KD curves in each model were the limit throat areas obtained from the same model itself. For the intermediate points ($P1$, $P3$, and $P5$), which are far from the limits, the inlet Mach number and throat area used were the ones derived from the full DS^2M model (*i.e.*, the same for all models).

For all cases shown in Fig. 8, no differences are observed between the results of the DS^2M-H model and the DS^2M model. However, it can be seen that, while there is a high level of agreement between all models for Mach numbers close to unity, particularly for $M^P_{N1}=1.01$, as the inlet Mach number increases, greater differences appear. In Fig. 8-(b) ($M^P_{N1}=1.10$), a significant deviation is observed in the results obtained with the DS^2M-F model compared to the others, becoming more pronounced for the IS and KD curves, where the DS^2M-F model predicts zero motion speed throughout the duct. Similarly, the DS^2M-S model begins to show noticeable differences from the DS^2M model in Fig. 8-(c), at an inlet entrance Mach number of $M^P_{N1}=1.20$.

Table 1
Duct throat areas considered in Eq. (69) for the five configurations given en Fig. 7, at each entrance Mach number.

Point	$\eta_t = A_t/A_1$	Comment: Position in Fig. 7
$P1$	$\eta_t\|_{IS} - 0.1\,(1-\eta_t\|_{IS})$	10% below IS curve
$P2$	$\eta_t\|_{IS}$	At IS curve
$P3$	$\frac{1}{2}\,(\eta_t\|_{IS} + \eta_t\|_{KD})$	Halfway between IS and KD curves
$P4$	$\eta_t\|_{KD}$	At KD curve
$P5$	$\frac{1}{2}\,(1+\eta_t\|_{KD})$	Halfway between KD and $A^*/A=1$ curves

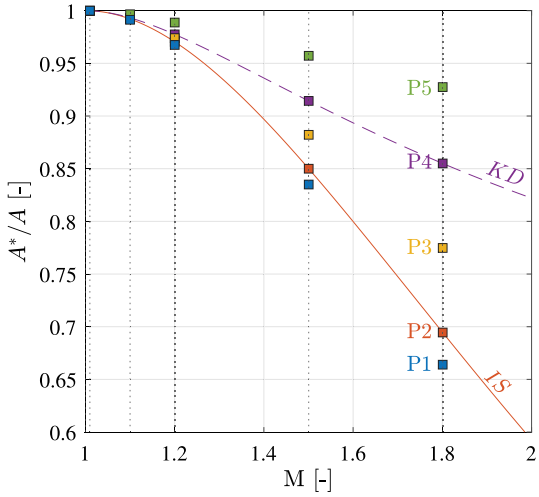

Fig. 7. Curves IS (solid line) and KD (dashed line), and selected points for results analysis. Vertical lines indicate inlet Mach numbers of M^P_{N1} = 1.01, 1.10, 1.20, 1.50, and 1.80.

According to Fig. 8-(c) ($M^P_{N1}=1.20$), there are significant differences between the approximated (DS^2M-F and DS^2M-S) and full (DS^2M) models. These differences increase notably with higher Mach numbers. Therefore, the results from low-order models (DS^2M-F and DS^2M-S) are omitted for higher Mach numbers. Instead, Fig. 9-(a) and 9-(b) present the shock wave motion speed, m^P_{Ns}, obtained using the DS^2M model and the **Method 3** of the DS^2M-H model for inlet entrance Mach numbers of $M^P_{N1}=1.50$ and 1.80, respectively. These results are also normalized to the maximum value achieved by the DS^2M model, $m^P_{Ns}|_{max}$. In these figures, even for an inlet entrance Mach number of $M^P_{N1}=1.50$, the results obtained with **Method 3** of the DS^2M-H model reasonably match those of the DS^2M model. However, for higher values, discrepancies become quite noticeable (see Fig. 9-(b)).

To complete the information presented in Figs. 8 and 9, the variation of the maximum shock wave motion speed, $m^P_{Ns}|_{max}$, obtained using the DS^2M model as a function of the inlet entrance Mach number, M^P_{N1}, is shown in Fig. 10. The maximum shock wave motion speed considered in each case is the one that appears at the throat in the conditions (Mach number and throat-to-entrance area ratio) defined by the $P5$ points from Fig. 7 and Table 1. In this figure, a monotonic growth can be observed. This growth is quite linear for inlet entrance Mach numbers close to unity, but deviates from linearity as the inlet entrance Mach number increases. This can be associated with an increase in the dynamic pressure of the upstream flow, leading to a stronger shock wave, both during its expulsion and swallowing, and an increase in motion speed.

The points of maximum speed occur at the throat (see Eq. (33)) and correspond to points $P5$ in Fig. 7 (above the KD limit). In addition, the larger the duct section areas (that is, more similar to A_1), the lower

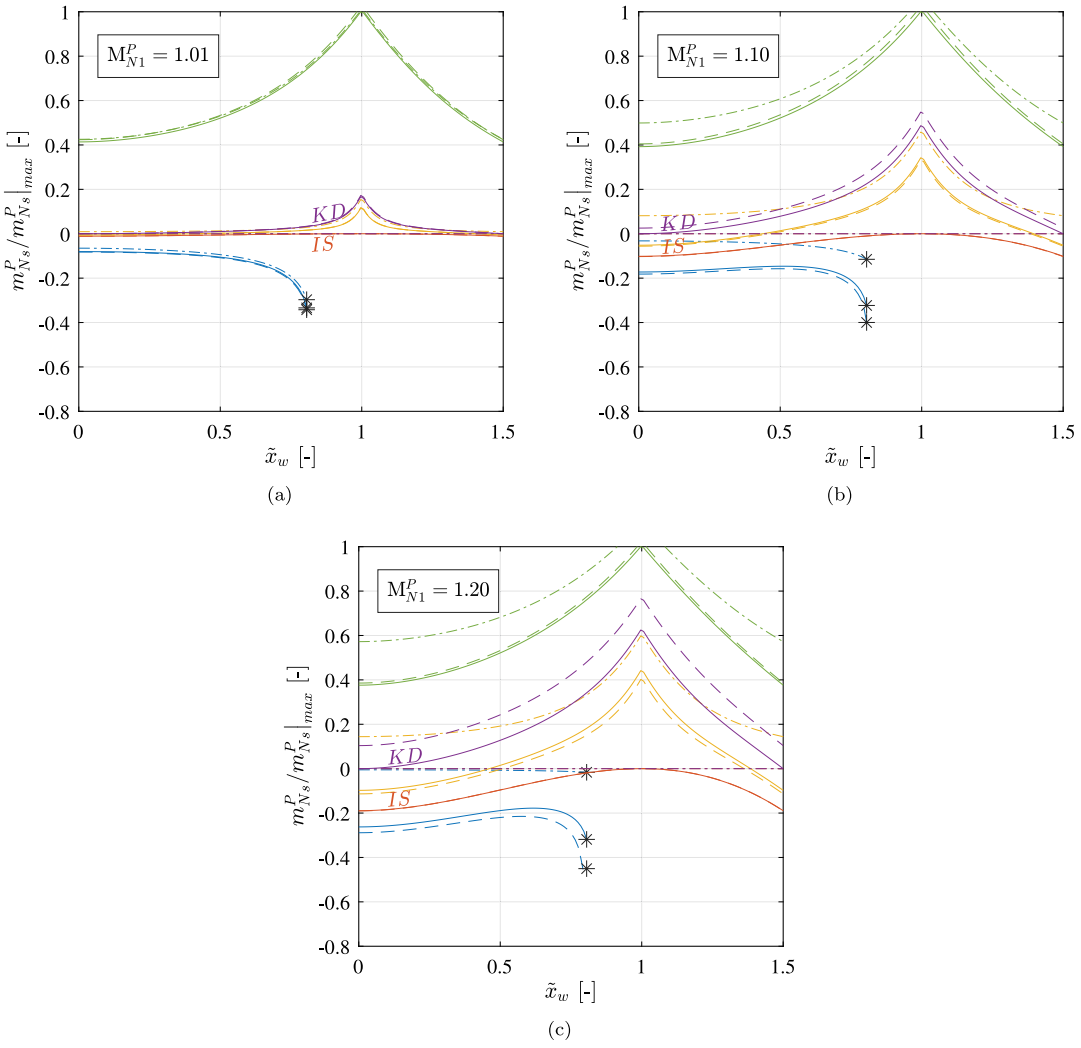

Fig. 8. Variation of the dimensionless shock wave motion speed, $m^P_{Ns}/m^P_{Ns}|_{max}$ (see Fig. 10), as a function of position, $\tilde{x}_w$, for an inlet entrance Mach number $M^P_{N1} = 1.01$ (a), 1.10 (b), and 1.20 (c); for the cases indicated in Fig. 7: $P1$, below the IS curve (blue); $P2$, on the IS curve (orange); $P3$, between the IS and KD curves (yellow); $P4$, on the KD curve (purple); and $P5$, above the KD curve (green). Results obtained using the DS^2M and DS^2M-H models (solid line), the DS^2M-F model (dotted–dashed line), and the DS^2M-S model (dashed line). (For interpretation of the references to color in this figure legend, the reader is referred to the web version of this article.)

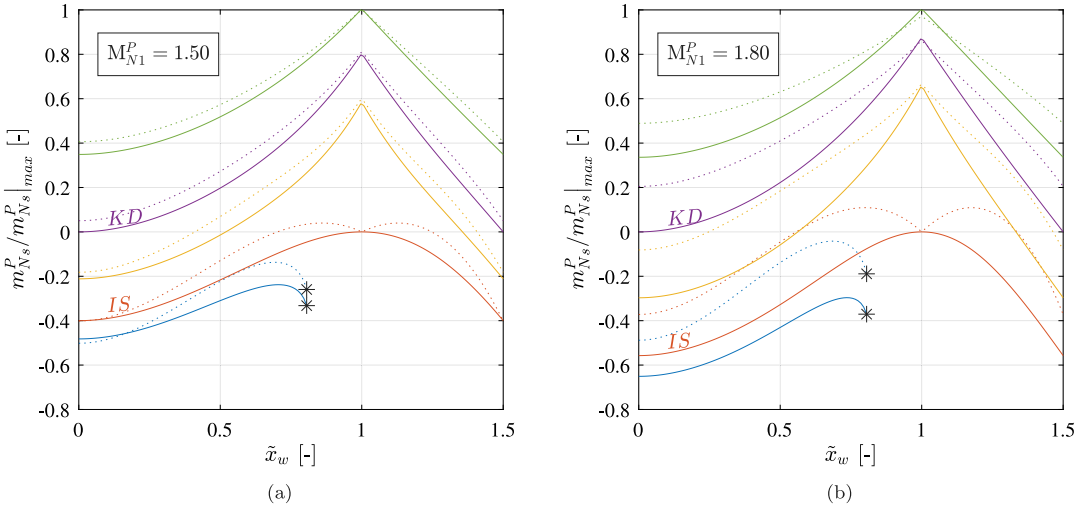

Fig. 9. As in Fig. 8 for $M^P_{N1} = 1.50$ (a) and 1.80 (b). Results obtained using the DS^2M model (solid line) and **Method 3** of the DS^2M-H model (dotted line).

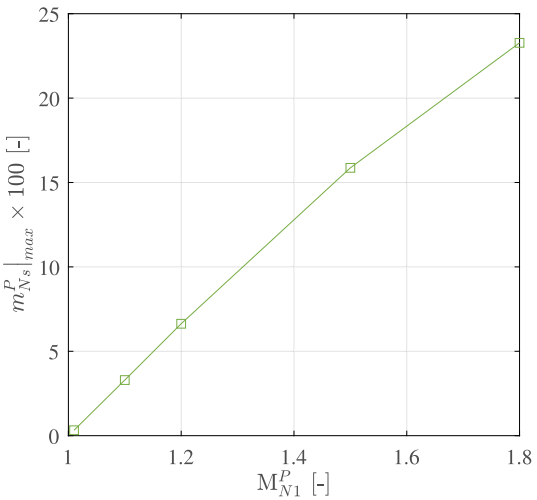

Fig. 10. Variation of the maximum dimensionless shock wave motion speed, $m^P_{Ns}|_{max}$, as a function of the inlet entrance Mach number, M^P_{N1}, for the different cases considered (see points $P5$ in Fig. 7 and Table 1). Results obtained using the DS^2M model.

the deceleration experienced by the flow and, therefore, the greater the shock wave motion speed.

At $P1$ points, the limit ($*$) can be reached in a given section and, from that position on, the curve finishes. This limit corresponds to $M_w \equiv 1$ and $A_w \equiv A^*$. Therefore, no solutions exist for smaller areas. No shock wave can appear at the right side of this limit point ($*$) and, if it appears on the left side, then it would have negative motion speed, and it would be expelled.

The physical interpretation of the observed differences between the simplified models becomes clearer when considering the assumptions underlying each approach. The $DS^2M - F$ model, which assumes only first-order perturbations, fails to capture the growing influence of geometry on shock wave dynamics as the Mach number increases. This also explains the model's prediction of zero motion speed in limiting cases (like on the IS or KD curves). In contrast, the $DS^2M - S$ model better incorporates the effects of geometry, but still omits higher-order terms that become increasingly relevant at moderate-to-high Mach numbers.

Physically, these discrepancies can be understood by examining the role of the pressure gradients induced by area variations. At low Mach numbers, changes in duct geometry cause relatively gentle pressure perturbations, allowing all models to converge in their predictions. However, as the flow speed and compressibility rise with Mach number, even small area variations near the throat induce strong pressure forces capable of accelerating or decelerating the shock wave significantly. This is especially true near the IS and KD limits, where flow stability is sensitive to small perturbations. The full DS^2M model, which includes the effects of dynamic wave interaction and geometry coupling, is thus better equipped to capture these nuances, especially when nonlinear behavior becomes dominant.

3.1. Comments on the influence of viscous effects

In real experimental tests, even in the purely mechanical problem studied (excluding effects such as mass addition or the presence of a combustion chamber) viscous phenomena, such as boundary layers, are nonetheless present. These viscous effects can be qualitatively accounted for by considering them as an effective reduction in the cross-section area for the flow within the duct under consideration. In particular, near the throat regions, the presence of boundary layers can effectively reduce the cross-section area at those locations. This reduction tends to promote unstart and hinder start in real inlets, requiring larger increases in area than those predicted theoretically to achieve start. It also leads to unstart at slightly larger areas than those estimated in the developed simplified models.

For a more in-depth analysis of how viscous effects can be incorporated into the developed formulation, and how such techniques can be used to compare with experimental results, the interested reader is referred to Carbajosa et al. [13].

4. Conclusions

In this work, three approximated models (valid when $M \approx 1$), derived from the DS^2M model proposed by Carbajosa et al. [13], have been developed with the aim of simplifying the analysis of shock wave motion in supersonic and hypersonic air inlets. In these cases, even for high Mach numbers, after an initial set of oblique shock waves, the normal shock wave that finally decelerates the flow from supersonic to subsonic regime is usually subjected to a Mach number close to unity and is positioned in the proximity of the throat, at least in the configurations close to the shock wave swallowing and expelling limits (KD and IS, respectively). In these cases, the proposed approximated models are applicable by considering an equivalent corrected Mach number in a given known section area. These approximated models provide analytical expressions that allow for the rapid evaluation of shock wave motion speed, as well as the determination of equilibrium positions, stability, and facilitate the description of the influence of key design parameters (such as the Mach number and cross-section area of the reference section, the critical area of the reference flow, the throat area, or the shock wave position).

The results obtained show that predictions of the approximated model align well with those of the full model within a Mach number range close to unity. However, as the Mach numbers increase, the discrepancies between the results of the approximated models and the full model also increase. As expected, the simplest model (the $DS^2M - F$) exhibits the greatest deviations compared to the full model, while the successive models ($DS^2M - S$ and $DS^2M - H$), which are more complex, show greater accuracy in approaching the full model solution.

The analytical expressions allow for the identification of the dependency of motion speed on the inlet entrance area, throat area, and the area of the section where the shock wave is located. In particular, according to the first order approximation, the sign of the motion speed depends on $(A_t - A^{P*})$. If the throat area is larger than the critical area of the incoming flow, the motion speed is positive, and the shock wave moves towards the throat. If the throat area is made smaller than the critical area of the incoming supersonic flow (no shock wave in the duct), then a shock wave appears at the throat, and, since the motion speed is negative, moves towards the entrance. The intensity of the motion speed follows $\left(A_w - A_t\right)^{-1/2}$, where $A_w > A_t$, from which it is deduced that the maximum velocity will be reached at the throat (where the area is minimal). Note that the shock wave motion speed intensity tends to infinity if $A_w \to A_t$, where the first order approximated model provides invalid results. Additionally, it is noteworthy that the results obtained using the $DS^2M - H$ model are very close to those of the DS^2M model, even for relatively high Mach numbers (around $M^P_{N1} = 1.50$), which is consistent with expectations for an asymptotic method.

In practical terms, the approximated models developed are particularly useful in the preliminary design stages, where simplicity and calculation speed are key factors. However, for operating conditions further from the validity range of the simplified models, it is recommended to use the DS^2M model or more advanced numerical tools to ensure the required accuracy. Overall, this work extends the capabilities of the DS^2M model, providing versatile tools for preliminary analysis and establishing clear limits for the applicability of the proposed approximations.

It can be observed that shock wave swallowing speeds are consistently higher than expelling speeds. Furthermore, maximum swallowing speeds and minimum expelling speeds occur at the throat. In the considered range ($M^P_{N1} \leq 1.80$), the maximum dimensionless shock wave motion speed, $m^P_{Ns}|_{max}$, remains small (necessary for the validity of the DS^2M model), indicating that the shock wave motion speed is substantially lower than the sound speed. Since all the temperatures are of the same order of magnitude, it does not matter to which temperature the sound speed is referred. A fraction of this sound speed can be used as an order-of-magnitude value to estimate shock motion speed in preliminary design phases.

CRediT authorship contribution statement

Carlos Carbajosa: Writing – review & editing, Writing – original draft, Validation, Software, Methodology, Investigation, Formal analysis, Data curation, Conceptualization. **Ángel Sanz-Andrés:** Writing – review & editing, Writing – original draft, Supervision, Project administration, Methodology, Investigation, Formal analysis, Conceptualization. **Alejandro Martínez-Cava:** Writing – review & editing, Supervision, Resources, Project administration, Funding acquisition, Conceptualization. **Sergio Marín-Coca:** Writing – review & editing, Visualization, Supervision, Conceptualization. **Sebastián Franchini:** Writing – review & editing, Supervision, Resources, Project administration, Funding acquisition.

Declaration of Generative AI and AI-assisted technologies in the writing process

During the preparation of this work the authors used ChatGPT in order to improve the translation and readability of the document. After using this tool, the authors reviewed and edited the content as needed and take full responsibility for the content of the published article.

Declaration of competing interest

The authors declare that they have no known competing financial interests or personal relationships that could have appeared to influence the work reported in this paper.

Acknowledgments

This work is part of the project TED2021-130541B-C21, funded by MCIN/AEI/10.13039/ 501100011033, the European Union "NextGenerationEU"/PRTR and project PID 2022-137630OB-C21 financed by MCIN/AEI/10.13039/ 501100011033/FEDER, UE. This research was supported by the FPU grant (Formación de Profesorado Universitario) FPU23/00716 from the Spanish Ministry of Science and Innovation (Ministerio de Ciencia, Innovación y Universidades) to Carlos Carbajosa.

Appendix A. Nomenclature

Superscripts

B	Subsonic branch.
m	Maximum speed condition.
P	Supersonic branch.
R	Supersonic or subsonic regime, depending on whether $R \equiv P$ or $R \equiv B$, respectively.
x	Method x (where $x = 1, 2,$ or 3) when using $DS^2M - H$ model.
z	Zero speed condition.

Subscripts

1	Inlet entrance.
d	Outgoing quantity evaluated in the shock wave reference frame.
F	Quantity referred to the $DS^2M - F$ model.
H	Quantity referred to the $DS^2M - H$ model.
IS	Quantity referred to the isentropic limit.
i	Incident quantity evaluated in the shock wave reference frame.
KD	Quantity referred to the Kantrowitz-Donaldson limit.
max	Maximum speed.
N	Quantity referred to the inlet reference frame.
n	Auxiliary index.
Pi	Quantity referred to the Point i.
S	Quantity referred to the $DS^2M - S$ model.
s	Total or stagnation quantity.
t	Inlet throat.
W	Quantity referred to the shock wave reference frame.
w	Shock wave position.

Greek symbols

δ	Incremental dimensionless area, $\eta - 1$.
ϵ_n	Auxiliary quantity for the nth term used in mathematical expansions.
η	Ratio between the area at a given section, A, and the area at the inlet entrance section, A_1.
γ	Specific heat ratio of air.
ε	Incremental Mach number, M − 1.
ξ	Area jump, $a^P - a^B$.
ζ	Throat deformation, $1 - \eta_t$.

Roman symbols

M	Mach number.
A	Area.
a	Incremental dimensionless area, $A/A^* - 1$.
$A*$	Critical area.
A_m, B_m, C_m	Coefficients of the quadratic equation for m^P_{Ns}.
C^M_n	Coefficient for the nth term in the Taylor series expansion of m^P_{Ns} obtained using the $DS^2M - F$ ($M \equiv F$), $DS^2M - S$ ($M \equiv S$), or $DS^2M - H$ ($M \equiv H$) model.
CR	Contraction ratio.
h^{Sx}_n	Coefficient for the nth term of the proposed approximated model for k^{Sx}_{A2}.
k_{M2}	Second-order coefficient of the Taylor series expansion of the Prandtl relation.
k_{A2}	Second-order coefficient of the Taylor series expansion of a.
k^{Sx}_{A2}	Second-order coefficient of the Taylor series expansion of a for the S branch using Method x (x=1, 2, or 3).
k_{A3}	Third-order coefficient of the Taylor series expansion of a.
k_{Tn}	Coefficient for the nth term in the Taylor series expansion of $\sqrt{T^P_{Ns}/T^P_w} + \sqrt{r_{Ts}}\sqrt{T_{Ws}/T^B_w}$.
L	Longitudinal distance between the inlet entrance and the throat.
l_{Tn}	Coefficient for the nth term in the Taylor series expansion of $\sqrt{T^P_{Ns}/T^P_w}$.

m^P_{Ns} Dimensionless motion speed of the shock wave scaled by the speed of sound at stagnation conditions, in the inlet reference frame.
R_g Gas constant for air.
r_{Ts} Ratio between T^P_{Ns} and T_{Ws}.
T Temperature.
x Longitudinal coordinate measured relative to the entrance section.
$\dot{x}$ Shock wave motion speed measured in inlet reference frame.
$\tilde{x}$ Dimensionless longitudinal coordinate, x, scaled by the quantity L.

Appendix B. Derivation of $\epsilon(a)$

The objective is to solve the problem of obtaining the incremental Mach number ϵ as a function of the incremental area a, *i.e.*, $\epsilon = \epsilon(a)$, starting from:

$$k_{A2}\epsilon^2 + k_{A3}\epsilon^3 \approx a. \tag{B.1}$$

To achieve this, ϵ is expanded as $\epsilon = \epsilon_0 + \epsilon_1$, where $\epsilon_1 \ll \epsilon_0$. Accordingly, Eq. (B.1) becomes:

$$k_{A2}\left(\epsilon_0^2 + 2\epsilon_0\epsilon_1 + \epsilon_1^2\right) + k_{A3}\left(\epsilon_0^3 + 3\epsilon_0^2\epsilon_1 + 3\epsilon_0\epsilon_1^2 + \epsilon_1^3\right) \approx a. \tag{B.2}$$

Given that $\epsilon_0^2 \gg \epsilon_0\epsilon_1 \gg \epsilon_1^2$ and $\epsilon_0^2 \gg \epsilon_0^3 \gg \epsilon_0^2\epsilon_1 \gg \epsilon_0\epsilon_1^2 \gg \epsilon_1^3$, the expression can be approximated to:

$$k_{A2}\epsilon_0^2 \approx a, \tag{B.3}$$

leading to:

$$\epsilon_0 \approx \pm\sqrt{\frac{a}{k_{A2}}}. \tag{B.4}$$

Moreover, substituting the above result into Eq. (B.2) and retaining the subsequent order terms, the following is obtained:

$$2k_{A2}\epsilon_0\epsilon_1 + k_{A3}\epsilon_0^3 \approx 0, \tag{B.5}$$

such that, considering the value obtained for ϵ_0:

$$\epsilon_1 \approx -\frac{k_{A3}}{2k_{A2}^2}a. \tag{B.6}$$

Finally:

$$\epsilon(a) \cong \pm\sqrt{\frac{a}{k_{A2}}} - \frac{k_{A3}}{2k_{A2}^2}a \tag{B.7}$$

Appendix C. Modeling of $k^P_{A2}(\varepsilon^P_{N1})$ and $k^B_{A2}(\varepsilon^P_{N1})$

To complete the improved approximated formulation, it is necessary to describe the model employed for $k^P_{A2}(\varepsilon^P_{N1})$ and $k^B_{A2}(\varepsilon^P_{N1})$. In this study, three possibilities have been analyzed:

1. *Method 1*: Maintaining the constant value k_{A2} obtained from the Taylor series expansion of Eq. (D.1). In this case, the coefficient values are:

$$k^{P1}_{A2}(\varepsilon^P_{N1}) = k^{B1}_{A2}(\varepsilon^P_{N1}) = k_{A2} = h^{R1}_0 = \frac{2}{\gamma+1} = \frac{5}{6} \simeq 0.833, \tag{C.1}$$

where the superscript indicates the method used to determine k_{A2}, and $R = P$ or B, depending on the case. Using this first method of the DS^2M-H model preserves the symmetry of the A(M) curve with respect to M = 1.

2. *Method 2*: Fitting the Mach number values contained within the interval $\varepsilon^B_n \in \left[-\varepsilon^P_{N1}, 0\right]$ for the subsonic branch and $\varepsilon^P_n \in \left[0, +\varepsilon^P_{N1}\right]$ for the supersonic branch is proposed. In this way, asymmetry is introduced. To do this, separate fits are given for each branch:

$$k^{R2}_{A2,n} = \frac{a(\varepsilon^R_n)}{\left(\varepsilon^R_n\right)^2}. \tag{C.2}$$

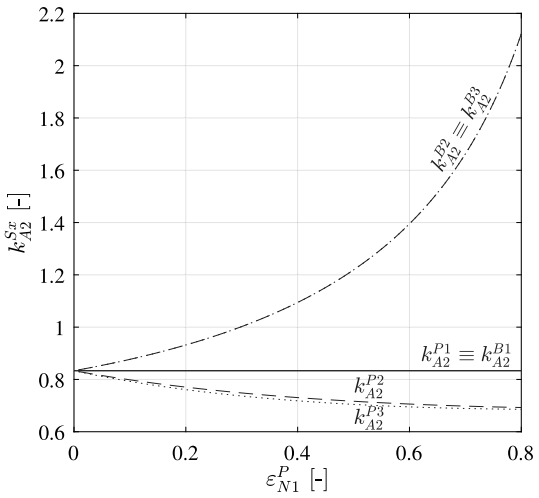

Fig. C.11. Functions $k^{Rx}_{A2}(\varepsilon^P_{N1})$, where $R \equiv P$ for the supersonic branch and $R \equiv B$ for the subsonic branch, and $x = 1, 2$, or 3, depending on the method used, as employed in the DS^2M-H model, for: **Method 1** (solid line), **Method 2** (dashed line), and **Method 3** (dotted line).

The value of k^{R2}_{A2} minimizing the mean squared error of $k^{R2}_{A2,n}$ is obtained. Subsequently, polynomial regression can be applied to provide $k^{R2}_{A2}(\varepsilon^P_{N1})$ values (with $R = P$ or B, as per the branch) as functions of ε^P_{N1}. By performing regression for values within the interval $\varepsilon^P_{N1} \in [0, 0.8]$ for each branch ($R = B$ or P), the following fittings are obtained:

$$k^{R2}_{A2}(\varepsilon^P_{N1}) \approx h^{R2}_0 + h^{R2}_1\varepsilon^P_{N1} + h^{R2}_2(\varepsilon^P_{N1})^2 + h^{R2}_3(\varepsilon^P_{N1})^3 + h^{R2}_4(\varepsilon^P_{N1})^4, \tag{C.3}$$

where the coefficients for the subsonic branch ($R = B$) are:

$$h^{B2}_0 \simeq +0.844,\ h^{B2}_1 \simeq +0.044,\ h^{B2}_2 \simeq +2.942,\ h^{B2}_3 \simeq -6.107,\ h^{B2}_4 \simeq +6.027, \tag{C.4}$$

while for the supersonic branch ($R = P$):

$$h^{P2}_0 \simeq +0.833,\ h^{P2}_1 \simeq -0.373,\ h^{P2}_2 \simeq +0.337,\ h^{P2}_3 \simeq -0.114,\ h^{P3}_4 = 0. \tag{C.5}$$

Comparing h^{R2}_0 and the subsequent coefficients reveals the asymmetry that appears in the DS^2M-F model. The hysteresis zone arises due to the lack of symmetry (see Fig. C.11).

3. *Method 3*: Finally, the best performance of the improved approximated formulation was observed when maintaining the value of $k^{B3}_{A2}(\varepsilon^P_{N1}) \equiv k^{B2}_{A2}(\varepsilon^P_{N1})$ provided by the adjustment in the previous section, while for $k^{P3}_{A2}(\varepsilon^P_{N1})$, the value was determined to provide an estimation of Eq. (5) at the inlet entrance, *i.e.*:

$$k^{P3}_{A2}(\varepsilon^P_{N1}) = \frac{a_1}{\left(\varepsilon^P_{N1}\right)^2}. \tag{C.6}$$

The above expression can be approximated as a third-order polynomial within the interval $\varepsilon^P_{N1} \in [0, 0.8]$, such that:

$$k^{P3}_{A2}(\varepsilon^P_{N1}) \approx h^{P3}_0 + h^{P3}_1\varepsilon^P_{N1} + h^{P3}_2(\varepsilon^P_{N1})^2 + h^{P3}_3(\varepsilon^P_{N1})^3, \tag{C.7}$$

where the coefficients take the values:

$$h^{P3}_0 \simeq +0.832,\ h^{P3}_1 \simeq -0.439,\ h^{P3}_2 \simeq +0.446,\ h^{P3}_3 \simeq -0.159. \tag{C.8}$$

The curves of $k^P_{A2}(\varepsilon^P_{N1})$ and $k^B_{A2}(\varepsilon^P_{N1})$ as functions of ε^P_{N1} for the three methods are shown in Fig. C.11.

Finally, the shock wave motion speeds obtained using the DS^2M model and the three methods of the DS^2M-H model for inlet entrance Mach numbers $M^P_{N1} = 1.10$ and 1.50 are shown in Fig. C.12. It can

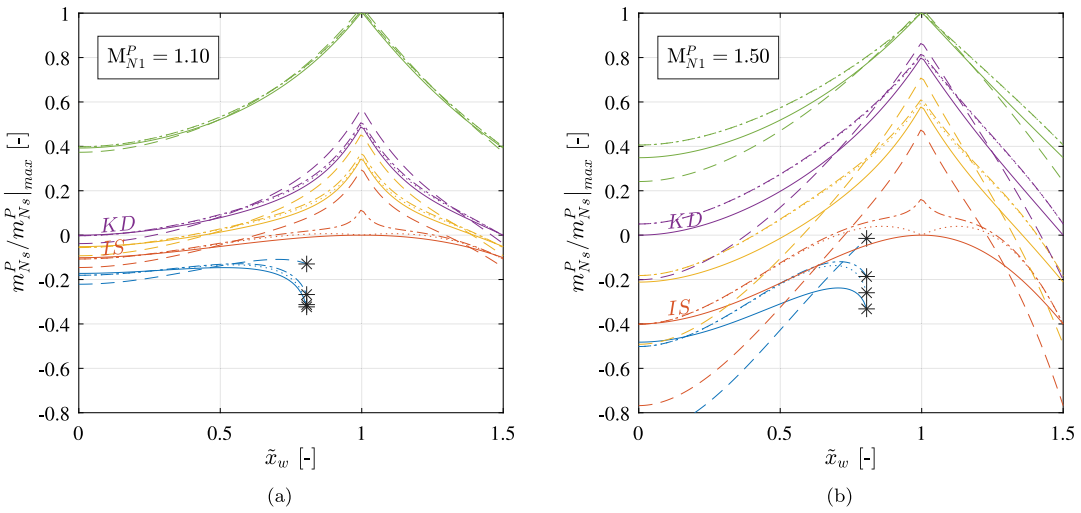

Fig. C.12. Variation with the dimensionless wave position, $\tilde{x}_w$, of the ratio between the dimensionless shock wave motion speed and its maximum value, $m^P_{Ns}/m^P_{Ns}|_{max}$ (see Fig. 10), for an inlet entrance Mach number $M^P_{N1} = 1.10$ (a), and 1.50 (b); for the cases considered in Fig. 7. These cases correspond to points: $P1$, below the IS curve (blue); $P2$, on the IS curve (orange); $P3$, between the IS and KD curves (yellow); $P4$, on the KD curve (purple); and $P5$, above the KD curve (green). Results are obtained using the DS^2M model (solid line) and the methods **Method 1** (dashed line), **Method 2** (dash-dotted line), and **Method 3** (dotted line) of the $DS^2M - H$ model. (For interpretation of the references to color in this figure legend, the reader is referred to the web version of this article.)

be observed that the **Method 3** of the $DS^2M - H$ model provides much closer results to the DS^2M model than the other two methods. Consequently, when comparing the models throughout the text, the results from **Method 3** of the $DS^2M - H$ model are consistently used.

Appendix D. Derivation of the motion speed coefficients using the $DS^2M - H$ model

With the considerations discussed so far, Eq. (5) can be approximated as:

$$a(\varepsilon) = \frac{A}{A^*}(\varepsilon) - 1 \approx k^R_{A2}(\varepsilon^P_{N1})\varepsilon^2, \tag{D.1}$$

where $R \equiv P$ in the supersonic branch, while $R \equiv B$ in the subsonic branch. Additionally, for a unitary Mach number at the inlet entrance (*i.e.*, $\varepsilon^P_{N1} = 0$), $k^P_{A2}(\varepsilon^P_{N1} = 0) = k^B_{A2}(\varepsilon^P_{N1} = 0) = k_{A2} = 2/(\gamma + 1) = 5/6$. Furthermore, the Prandtl relation given by Eq. (6) can be expanded as a series by assuming $M_i = 1 + \varepsilon_i$ and $M_d = 1 + \varepsilon_d$. Retaining terms up to the second order in ε_i, the following is obtained:

$$\varepsilon_d(\varepsilon_i) \approx -\varepsilon_i + k_{M2}\varepsilon_i^2, \tag{D.2}$$

where $k_{M2} = (3\gamma - 1)/(\gamma + 1) = 4/3$. The values of ε^P_{Nw} and ε^B_{Nw} are determined analogously to the first approximated formulation presented in this section, with appropriate modifications introduced in k_{A2}. Thus, Eq. (46) takes the form:

$$a_1 \approx k^P_{A2}(\varepsilon^P_{N1})\left(\varepsilon^P_{N1}\right)^2, \tag{D.3}$$

such that Eq. (19) becomes:

$$\varepsilon^P_{Nw} \approx +\sqrt{\frac{a^P_w}{k^P_{A2}(\varepsilon^P_{N1})}} = +\sqrt{\frac{\delta_w + a_1\eta_w}{k^P_{A2}(\varepsilon^P_{N1})}}. \tag{D.4}$$

Similarly, Eq. (21) assumes the following form:

$$\varepsilon^B_{Nw} \approx -\sqrt{\frac{a^B_w}{k^B_{A2}(\varepsilon^P_{N1})}} = -\sqrt{\frac{\delta_w - \delta_t}{k^B_{A2}(\varepsilon^P_{N1})\eta_t}}. \tag{D.5}$$

It can be verified that in Eqs. (D.4) and (D.5), both $|\varepsilon^P_{Nw}| \ll 1$ and $|\varepsilon^B_{Nw}| \ll 1$ are small, as they depend on the terms a, δ, and ε^P_{N1}, all of which are much smaller than unity. Expressing the Mach numbers before and after the shock wave in axes fixed to the inlet, M^P_{Nw} and M^B_{Nw}, respectively, in terms of ε^P_{Nw} and ε^B_{Nw}, the exact expressions derived by Carbajosa et al. [13] can be expanded as a series. The sequence is as follows:

1. From Eq. (9), the following relation is obtained:
$$T^P_{Ns}/T^P_w = T^P_{Ns}/T^P_w(\varepsilon^P_{Nw}). \tag{D.6}$$
2. Substituting the above result into Eq. (7), it is derived that:
$$M^P_{Ww} = M^P_{Ww}(m^P_{Ns}, \varepsilon^P_{Nw}). \tag{D.7}$$
3. Introducing the preceding result into Eq. (12), it is obtained:
$$r_{Ts} = r_{Ts}(m^P_{Ns}, \varepsilon^P_{Nw}). \tag{D.8}$$
4. Using the previous relations in Eq. (13), it is found that:
$$T_{Ws}/T^B_w = T_{Ws}/T^P_w(m^P_{Ns}, \varepsilon^P_{Nw}, \varepsilon^B_{Nw}). \tag{D.9}$$
5. Substituting the above results into Eq. (8):
$$M^B_{Ww} = M^B_{Ww}(m^P_{Ns}, \varepsilon^P_{Nw}, \varepsilon^B_{Nw}). \tag{D.10}$$
6. Finally, employing Eq. (14), an implicit equation is derived, relating:
$$m^P_{Ns}|_H = m^P_{Ns}(\varepsilon^P_{Nw}, \varepsilon^B_{Nw}). \tag{D.11}$$

At this stage, a highly nonlinear expression is obtained, involving only the quantities m^P_{Ns}, ε^P_{Nw}, and ε^B_{Nw}. Since these three quantities are small, a Taylor series expansion up to the second order can be performed for the wave motion speed, $m^P_{Ns}|_H$, as defined by Eq. (D.11). This results in a quadratic equation where the coefficients depend on the magnitudes ε^P_{Nw} and ε^B_{Nw}. Solving this equation and selecting the branch with zero motion speed for null values of ε^P_{Nw} and ε^B_{Nw}, it is obtained that:

$$m^P_{Ns}|_H(\varepsilon^P_{Nw}, \varepsilon^B_{Nw}) \approx C^H_1\left[\varepsilon^P_{Nw} + \varepsilon^B_{Nw}\right] + C^H_2\varepsilon^P_{Nw}\varepsilon^B_{Nw} + C^H_3\left[\left(\varepsilon^P_{Nw}\right)^2 + \left(\varepsilon^B_{Nw}\right)^2\right], \tag{D.12}$$

with $\varepsilon^P_{Nw} = \varepsilon^P_{Nw}(\tilde{x}_w; \varepsilon^P_{N1})$ and $\varepsilon^B_{Nw} = \varepsilon^B_{Nw}(\tilde{x}_w; \varepsilon^P_{N1})$ given by Eq. (65). In Eq. (D.12), the coefficients take the values:

$$C^H_1 \simeq +0.456,\ C^H_2 \simeq +0.228,\ C^H_3 \simeq -0.190 \tag{D.13}$$

References

[1] E.T. Curran, W.H. Heiser, D.T. Pratt, Fluid phenomena in scramjet combustion systems, Annu. Rm. Fluid. Mech 28 (1996) 18, http://dx.doi.org/10.1146/annurev.fl.28.010196.001543.

[2] S. O'byrne, M. Doolan, S.R. Olsen, A.F.P. Houwing, Analysis of transient thermal choking processes in a model scramjet engine, J. Propuls. Power 16 (5) (2000) 808–814, http://dx.doi.org/10.2514/2.5645.
[3] N. Mushtaq, P. Gaetani, Understanding and modeling unstarting phenomena in a supersonic inlet cascade, Phys. Fluids 35 (2023) http://dx.doi.org/10.1063/5.0160706.
[4] D.M. Van Wie, Scramjet inlets, in: Scramjet Propulsion, American Institute of Aeronautics and Astronautics, 2001, pp. 447–511, http://dx.doi.org/10.2514/5.9781600866609.0447.0511.
[5] J. Chang, N. Li, K. Xu, W. Bao, D. Yu, Recent research progress on unstart mechanism, detection and control of hypersonic inlet, Prog. Aerosp. Sci. 89 (2017) 1–22, http://dx.doi.org/10.1016/j.paerosci.2016.12.001.
[6] V.I. Zvegintsev, Gas-dynamic problems in off-design operation of supersonic inlets (review), Thermophys. Aeromechanics 24 (2017) 807–834, http://dx.doi.org/10.1134/S0869864317060014.
[7] J. Chang, Y. Fan, W. Bao, D. Yu, Y. Shen, Unstart margin control of hypersonic inlets, Acta Astronaut. 66 (1) (2010) 78–87, http://dx.doi.org/10.1016/j.actaastro.2009.05.021.
[8] J. Chang, R. Zheng, L. Wang, W. Bao, D. Yu, Backpressure unstart detection for a scramjet inlet based on information fusion, Acta Astronaut. 95 (2014) 1–14, http://dx.doi.org/10.1016/j.actaastro.2013.10.010.
[9] X. Jiao, J. Chang, Z. Wang, D. Yu, Hysteresis phenomenon of hypersonic inlet at high mach number, Acta Astronaut. 128 (2016) 657–668, http://dx.doi.org/10.1016/j.actaastro.2016.08.025.
[10] A. Kantrowitz, C. du P. Donaldson, Preliminary investigation of supersonic diffusers, Tech. Rep, (Adv. confid. report L5D20) NACA, 1945.
[11] H. xia Huang, H. jun Tan, F. bo Li, X. bin Tang, Y. Qin, L.B. Xie, Y.Y. Xu, C. min Li, S. min Gao, Y. Zhang, S. Sun, D. Zhao, A review of the shock-dominated flow in a hypersonic inlet/isolator, Prog. Aerosp. Sci. 143 (2023) http://dx.doi.org/10.1016/j.paerosci.2023.100952.
[12] J. Zhang, L. Lin, G. Luan, W. Bao, Experimental research on the stability margin of a variable geometry scramjet combustor in wide flight conditions, Acta Astronaut. 202 (2023) 151–156, http://dx.doi.org/10.1016/j.actaastro.2022.10.008.
[13] C. Carbajosa, Á. Sanz-Andrés, A. Martínez-Cava, M. Ogueta-Gutiérrez, Analysis of the unsteady shock wave motion in inlet unstart processes, Acta Astronaut. 234 (2025) 601–618, http://dx.doi.org/10.1016/j.actaastro.2025.05.006.
[14] Y. Jin, Y. Zhang, X. Li, H. Tan, S. Sun, Suppression of flow response hysteresis in the throttling/unthrottling process for supersonic inlet, Acta Astronaut. 202 (2023) 34–47, http://dx.doi.org/10.1016/j.actaastro.2022.09.052.
[15] C. Tao, Z. Lv, D. Yu, Multistability and complex routes of supersonic inlet start/unstart, J. Propuls. Power 27 (2011) 1204–1211, http://dx.doi.org/10.2514/1.B34235.
[16] A. Kantrowitz, The formation and stability of normal shock waves in channel flows, Tech. Rep., (Tech. Note 1225) NACA, 1947.
[17] G.B. Whitham, Linear and nonlinear waves, Wiley-Interscience, 1973, p. 636.
[18] Z. Han, X. Yin, Shock dynamics, vol. 11, Springer Netherlands, Dordrecht, 1993, http://dx.doi.org/10.1007/978-94-017-2995-6.
[19] R. Tahir, Analysis of Shock Dynamics in Supersonic Intakes (Ph.D. thesis), McGill, Montréal, Québec, Canada, 2008.
[20] K. Matsuo, Y. Miyazato, H.D. Kim, Shock train and pseudo-shock phenomena in internal gas flows, Prog. Aerosp. Sci. 35 (1999) 33–100, http://dx.doi.org/10.1016/S0376-0421(98)00011-6.
[21] T. Tamaki, Y. Tomita, R. Yamane, A study of pseudo-shock, Bull. the JSME 13 (55) (1970) 51–58, http://dx.doi.org/10.1299/jsme1958.13.51.
[22] J.L. Wagner, K.B. Yuceil, A. Valdivia, N.T. Clemens, D.S. Dolling, Experimental investigation of unstart in an inlet/isolator model in mach 5 flow, in: AIAA Journal, 47, 2009, pp. 1528–1542, http://dx.doi.org/10.2514/1.40966.
[23] A. Pathak, P. Khare, V. Kulkarni, Impact of energy deposition as active flow control on scramjet inlet performance using immersed boundary method, Acta Astronaut. 224 (2024) 291–308, http://dx.doi.org/10.1016/j.actaastro.2024.08.023.
[24] J. Kang, F. Song, Y. Wu, D. Zhang, J. Zhou, X. Sun, Experimental study on the suppression of inlet blockage in rotating detonation combustor by porous-wall, Acta Astronaut. 225 (2024) 477–488, http://dx.doi.org/10.1016/j.actaastro.2024.09.030.
[25] F. Gnani, H. Zare-Behtash, K. Kontis, Pseudo-shock waves and their interactions in high-speed intakes, Prog. Aerosp. Sci. 82 (2016) 36–56, http://dx.doi.org/10.1016/j.paerosci.2016.02.001.